Under-Ice Fluid Dynamics in Freshwater Lakes: Implications for Ecology in a Changing Climate

by

Taylor Hanson

A thesis
presented to the University of Waterloo
in fulfillment of the
thesis requirement for the degree of
Master of Mathematics
in
Applied Mathematics

Waterloo, Ontario, Canada, 2021

Author's Declaration

I hereby declare that I am the sole author of this thesis. This is a true copy of the thesis, including any required final revisions, as accepted by my examiners.

I understand that my thesis may be made electronically available to the public.

Abstract

An abundance of evidence exists to support the notion of annual winter blooms of phytoplankton, particularly diatoms, persistent in the surface waters of freshwater lakes located in temperate and boreal climatic zones. Non-motile diatoms are at the mercy of movements within the water column. Under ice cover, the distribution of solar radiation across the lake surface drives convective motions that work to push phytoplankton out of the photic zone; this is the region of the water column that harbors sufficient light conditions for photosynthesis and growth. Winter conditions determine proceeding phytoplankton populations and as such, changes to the mixing and circulation regimes under ice cover may alter blooms in the subsequent open water seasons. Physical fluid processes in winter are controlled by climatic forcing. Thus, it is anticipated that with climate change, freshwater ecosystem compositions will be influenced.

In this thesis, we use a non-hydrostatic, pseudospectral model, coined SPINS, to resolve under-ice fluid dynamics driven by incoming solar radiation. More specifically, we employ a three band radiation model to determine how variations in the absorption of incoming solar radiation affect the distribution of phytoplankton beneath the ice surface in late winter (early spring). We consider four cases to identify how changes to the initial temperature stratification and the under-ice irradiance (light levels) affect coupled bio-physical processes occurring within the water column over different time scales. Two separate sites are considered, Lake Erie and Lake Onego, to quantify the effects of radiatively driven convection in lakes with differing optical environments. This work suggests that small differences in water temperatures and weather conditions can cause significant variations to under-ice fluid processes that impact phytoplankton development. This observed sensitivity of hydrodynamics implies that climate change is likely to affect winter mixing regimes.

Acknowledgements

First and foremost, I would like to thank my supervisor Marek Stastna, who always had (or found) an answer to my never-ending stream of questions. Zoom is not my preferred method of communication yet you always made yourself available and for both your time and shared knowledge, I am grateful. On that note, I must also acknowledge my fluid lab mates who were always willing to help with research problems or make me laugh; whichever I needed most that day. My time in Waterloo was much too short but I am glad that it was spent in your company. Additionally, to my thesis committee members, Francis Poulin and Michael Waite, thank you for agreeing to review my work.

Thank you to my family, especially my wonderful parents. I cannot imagine it was easy to adopt a stressed graduate student back into the (empty) nest following a nation-wide lockdown. Nevertheless, I appreciate everything you have done and continue to do for me. I would not be where I am today without your love and support. Of course, there is also my sister who always knows exactly what to say (or do) to lift my spirits. I am so grateful to have the relationship I do with you.

To all of my friends, near and far, thank you for always being there for me. You always know when distraction is necessary and I look forward to many more now that this thesis is all wrapped up. In particular, I would like to single out Keenan. You have been my biggest supporter throughout this process, despite not fully understanding what it is that I have been working on. Thank you for all the encouragement and happiness you give me.

Dedication

To my best friend, Keenan. Words cannot express what you mean to me. On second thought, neither will the content of this thesis, but please accept the intended flattery.

Table of Contents

List of Figures

List of Tables

Chapter 1

Introduction

1.1 Impacts of Climate Change: Ice Cover and Lake Ecology

Climate change influences freshwater ecosystems. Understanding this influence, however, poses great challenges given the myriad of pathways within an ecosystem and the spatial variability that exists on numerous scales. Lakes constitute a majority of the Earth's liquid freshwater supply in addition to supporting enormous biodiversity. The sensitivity of lakes, specifically to climate change, make them effective indicators of change [2]. That is, the physical, chemical, and biological properties of lakes are easily measurable and thus comparable over both space and time. Some climate related response variables include water temperature, dissolved organic carbon (DOC) (interchangeable with dissolved organic matter (DOM): DOC refers specifically to the carbon in DOM [25]) and the composition of primary producers. Dissolved organic matter (DOM) constitutes the largest organic carbon pool in the water column and integrates many ecosystem responses within the lake, including heat absorption and lake metabolism (microbial activity) ([65], [2]). Perhaps water temperature, with its ties to thermal stratification, is the most important indicator. The underlying thermal structure of lakes controls mixing dynamics, affecting nutrient and oxygen exchange throughout the water column, which in turn determines the vertical distribution and composition of primary producers. Recent studies support evidence that lakes worldwide have been transitioning, with shifts tending towards warmer surface water temperatures, extended ice-free periods, alongside altered thermal stratification [22]. Understanding the biological implications of these altered physical states has become a ripe area of research for ecologists.

Most studies of freshwater aquatic ecosystems have focused on the effects of a changing climate to open-water conditions, as experienced in late spring, summer, and early autumn. One example is provided by the study of O'Reilly et al. [44], who found that summer surface water temperatures across a series of global lakes are rising alarmingly fast. This has numerous (negative) consequences, including increased harmful algal blooms (HABs), as well as heightened evaporation, or reduced water levels, to name a few. These warming trends are not unique to the warmer months, however, as winter ice cover plays a major role in determining the characteristics of these trends. Increased air temperatures have led towards a shortened ice-covered period, or no ice cover at all [41]. Magnuson et al. [40] revealed reduced ice cover across lakes in the Northern Hemisphere, associated with later freeze and earlier break-up dates. Changes in the ice-covered period directly affect ecosystem services provided by freshwater ([56], [39]). For example, some communities rely on seasonally ice-covered lakes for transportation and tourism, meaning that less ice reveals more economic challenges. As long-term climate change alters environmental conditions, with effects cascading between seasons, it becomes increasingly important to extend our study of freshwater ecosystems into the winter months.

Despite the urgent need to extend our efforts between seasons ([39], [24]), relatively little is known of winter freshwater ecology. The historical research focus on the summer 'growing' season has led to the misconstrued notion of winter as a quiescent period. Even when blanketed with snow and ice, aquatic ecosystems are capable of high productivity. This fact has been demonstrated in marine ecosystems, which provide compelling evidence that winter conditions are far from inactive [3]. Freshwater research is behind that of marine research as it pertains to under-ice ecology. In fact, a recent study suggests that only 2% of the peer-reviewed freshwater literature has extended their efforts to include under-ice processes [24]. A large number of lakes situated in high latitude countries, or more specifically, those located in the temperate and boreal climatic zones, are seasonally covered by ice for more than 40% of the year [5]. It is these Northern ecosystems that are expected to experience the highest rates of change in the coming years [16]. Complications undoubtedly arise regarding sample collection in the winter months, issues of safety being the utmost concern, coupled with logistical challenges. However, this does not explain why most studies of lake ecosystems tend to omit this time frame completely, especially when one considers the severity of the situation at these latitudes.

Our current understanding of the under-ice environment in freshwater lakes suggests conditions characterized by low and relatively constant temperatures, reluctant water movements, and limited light availability. Furthermore, ice acts as a barrier to external forcing, reducing both sediment resuspension (due to over-water wind) and gas exchange with the surrounding atmosphere (the latter having serious implications for winter anoxia) [5].

Thus, ice cover largely impacts the underlying physical processes of lakes, which in turn influences the ecosystem processes. The physical processes of greatest interest tend to center around the dynamics of temperature, light, and mixing, all of which are reduced with the onset of ice cover. The formation of ice naturally requires lower temperatures, while the accumulation of snow on its surface reduces light flux to the water column. There is variability in this light flux however, as snow is swept away by wind or melts, thereby increasing light penetration to the water column which eventually causes mixing [39]. As seasonally ice-covered lakes respond to climatic changes, the lakes themselves may become more dynamic [11] which hosts serious consequences for primary producers.

1.2 Primary Producers (Phytoplankton)

Primary producers are the base that supports overlying levels of lake biota, and as such, the primary productivity of lakes is dependent on their health and distribution. Note that the primary productivity of a lake refers to the productivity of the photosynthesizers to absorb nutrients from the water and energy from sunlight in order to supply oxygen to the water column. Aquatic algae are microscopic (non-vascular) plants that contain chlorophyll and grow by photosynthesis; they come in countless forms and live in nearly all kinds of environments. Freely suspended algae are commonly referred to as phytoplankton [27], though freely is perhaps a misnomer; often they are unable to move by themselves, but are instead at the mercy of movements in the water column. Primary consumers, such as zooplankton, can move freely throughout the water column and feed on phytoplankton [27].

Phytoplankton are frequently employed as indicators of climate change within freshwater ecosystems given their rapid response to subtle changes in the water column, specifically thermal changes. Although relatively short-lived, the abundance and composition of phytoplankton communities in many lakes has been well-documented [2]. Measurements often indicate the concentration of chlorophyll-a, a pigment common to all groups of phytoplankton allowing them to perform photosynthesis [27]. These measurements provide a reasonable estimate of the algal biomass in a given lake and their records are useful for extracting climate-related changes over time.

Past observations hint that environmental factors affect the competitive advantage of phytoplankton taxa, leading to shifts in the community structure [60]. The biological characteristics of a lake are closely coupled to the physical characteristics of the water column, where changes in nutrients, light, mixing, and thermal stratification are generally most important ([27], [1], [33]). Note that phytoplankton populations have varying susceptibilities to grazing by zooplankton as well, though we ignore this level of detail in the current work.

As conditions in the lake change over time (and even more so in our changing climate), certain species will be eliminated due to their inability to adapt to the new environment, whereas planktonic groups with adaptations favourable to the conditions will thrive. This species 'turnover' represents an important ecological pattern in freshwater lakes known as algal succession [27]. For example, in the summer months, bloom-forming cyanobacteria, or blue-green algae, tend to dominate over other phytoplankton groups. This helps to explain why harmful algal blooms (HABs) typically occur when water temperatures are higher. Taxonomic groups that are especially sensitive to mixing, with adaptions toward lower light and temperature conditions, tend to dominate earlier in the spring [2].

Changes to the ice-covered period in lakes undoubtedly influences algal succession. However, the effects of these changes are not well understood, nor are the more general effects of winter conditions as they relate to the starting point in the yearly succession of phytoplankton community structure ([5], [1]). Ice affects phytoplankton communities in various ways. The ice itself can provide a potentially vast habitat for phytoplankton [23], where in some ecosystems, large under-ice blooms occur [39]. Variations in ice and snow cover have a profound impact on the rates of primary productivity as well. The unique low light environment under ice cover is associated with reduced turbulence, leading to vertical gradients in temperature, oxygen and nutrients. Changes to the structure, composition and duration of the ice cover will affect these under-ice (stratification) patterns, and similarly, which species of phytoplankton are most likely to survive. The resident species at ice-off will serve as an inoculum for the ice-free season, influencing the successional pattern of algae in the late spring, and possibly, the entire year ([1], [5], [54]). Thus, it is likely that winter conditions determine proceeding phytoplankton populations and as such, changes in ice cover and surrounding climatic conditions (winter precipitation) may alter blooms in the subsequent open water seasons ([39], [24]). Hence, our understanding of the lake function in subsequent seasons is limited by our comprehension of phytoplankton and nutrient dynamics in the winter months.

If we would like to consider winter as the starting point in the yearly algal succession, it is important to know which phytoplankton group is persistent in the ice-covered waters of temperate lakes. In a study of Lake Erie conducted over the period of four years, Twiss et al. [54] consistently noted the presence of diatoms (specifically, *Aulacoseira islandica*) in the water column situated directly beneath the ice. This research provided an abundance of evidence to support the notion of annual winter blooms of diatoms persistent in surface waters throughout the season. Further to this, diatom blooms may frequently occur under the ice of other lakes as well, so long as the ice- and snow-cover conditions allow for enhanced light availability near the surface (this establishes mixing conditions conducive to diatom growth). Similar blooms of the diatom, *Aulacoseira islandica*, in Lake Baikal,

Russia ([33], [31], [21]) and Lake Onego, Russia [52] have been observed.

Diatoms are a phylum of non-motile unicellular algae, with individual cells typically in the size range of 10-200μm ([60], [47]). The cells themselves have dense walls, and this coupled will their overall size, lead them to sink readily in the water column. Further to this, diatoms are generally well-adapted to low light levels as compared to other phytoplankton taxa, and have comparatively high growth rates if encountering suitable conditions [47]. The interplay between turbulent mixing and access to light limits the temporal and spatial range able to sustain diatom growth. In lakes susceptible to seasonal ice cover, diatom populations are most profound in late winter/early spring when radiatively induced mixing is able to suspend them in the (relatively) well-lit upper regions of the water column [60]. Despite the cold temperatures encountered beneath ice cover, diatoms are able to photosynthesize actively and thus have a competitive advantage in the cold season of most high latitude lakes, lending to them being the representative species at this time ([64], [52]).

Given that diatoms are heavily reliant on mixing as a suspension mechanism, the physical and thermal dynamics of the water column are extremely important to their survival. Both thermal stratification and physical mixing processes are controlled by climatic forcing, and thus, it is anticipated that with climate change, diatom community structure will be harder to predict in the future [60]. This is in part due to intensified stratification, as a result of reduced ice cover, and habitat loss (recall that blooms often form attached to the ice-surface). Although diatoms as a species may be able to adapt to this climate-induced 'super' stratification by selecting smaller sized diatoms with lower sinking rates ([60], [22]), it is most probable that diatoms will be replaced by other phytoplankton (taxonomic) groups that are best suited to environments with reduced mixing, such as cyanobacterial blooms ([11], [22]). In other words, a warming climate lends itself to select for species that are able to maintain their vertical position in the upper water column, increasing access to light.

1.3 Radiatively Driven Convection

The most consequential pathway in which climate change affects phytoplankton is through the modification of the lake's thermal structure. Stratification is vital to primary producers as it provides a means to regulate the distribution of nutrients, thereby determining where phytoplankton can thrive. The under-ice environment in temperate and cold-climate lakes is characterized by a pattern of inverse thermal stratification, with the coldest temperatures located right beneath the ice surface, transitioning to a warmer, more dense layer below. The ice-water interface hovers near the freezing point, while the under-ice waters

are typically colder than, but approach the temperature of maximum density, $T_{md} \approx 4°C$ for freshwater ([34], [5], [33]). The ice cover acts as a lid against external forcing, effectively reducing wind driven mixing. Thus, under-ice hydrodynamics are predominately density-driven processes, resulting due to changes in temperature ([5], [9]). Salinity differences also drive changes in density, but are generally negligible in freshwater environments, as will be considered in this thesis.

It is well known that the equation of state for temperature stratified water is non-monotonic in the cold water regime ([50], [56], [5]). The temperature of maximum density is denoted by T_{md} with a corresponding density $\rho_{max} = \rho(T_{md})$ in Figure 1.1. The $\rho(T)$ curve near T_{md} is essentially quadratic, meaning that water becomes less dense at both higher and lower temperatures. The blue shaded region of Figure 1.1 corresponds to the region of interest in under-ice environments. The typical density differences in the cold water regime are small. For example, an increase in water temperature from 2°C to 2.5°C results in a density difference approximately 2.5 times larger than the same 0.5°C increase starting from an initial temperature of 3°C [50]. Thus, only small temperature differences are required to drive fluid motions under the ice. For a large part of the winter, snow cover on the lake surface reflects a significant portion of incident solar radiation. However, as the solar insolation strengthens after the winter solstice, especially early in the springtime, the snow cover melts and the ice surface allows light to penetrate through to the water column below, heating up the near-surface waters. As a consequence of the nonlinear equation of state, this warming increases the density of water near the freezing point, leading to gravitational convective instabilities ([56], [8], [4], [19]). With time, the depth of convection increases as does the temperature of the deeper water layers ([50], [42]). Note however, that heating of water at the temperature of maximum density, T_{md}, does not increase its density nor lead to the excitation of under-ice instabilities [56]. This sensitivity within a narrow range of temperatures means that under-ice flow dynamics are particularly susceptible to changes in climate.

Hence, the two major factors determining the hydrodynamics of lakes following the formation of ice cover are the underlying pattern of inverse thermal stratification, coupled with the fact that the ice and snow cover insulate the water column from atmospheric heat and momentum fluxes for the better part of the season. The remaining drivers of under-ice fluid motions include heat flux from the sediments and solar radiation penetrating through the ice surface leading to convective currents [34]. Mixing in ice-covered lakes can be additionally caused by oscillations of the ice cover (induced seiching), or by through-flow currents such as from rivers or melt water ([34], [4], [42]). For the purpose of this thesis, we restrict our attention to the importance of the two former energy supply mechanisms, which vary over the course of the ice-covered period. In fact, most seasonally ice-covered

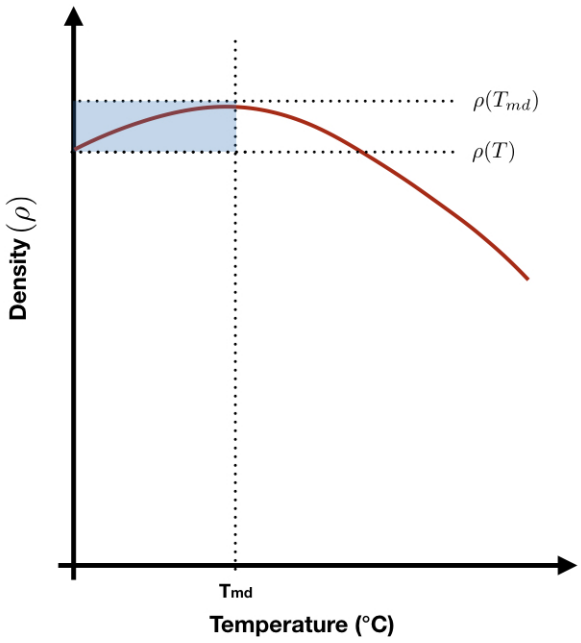

Figure 1.1: The density of freshwater as a function of temperature. The temperature of highest density, approximately $4°C$, is labelled T_{md}. The range of densities experienced between the freezing point, T, and temperature of maximum density is shaded in blue.

lakes reveal a two-stage temporal pattern, which lends itself to the characterization of two distinct phases: Winter I and Winter II ([34], [5]).

Winter I occurs earlier in the season and is characterized by the layer of snow cover on the ice-surface which insulates the lake from solar radiation. In this phase, under-ice mixing processes are predominantly due to heat flux from the sediment, leading to density driven currents near the lake bed (see Figure 1.2 (a)). Heat release from the sediment is thought to be an important driver for circulation and mixing in small, shallow lakes, but its effects are less pronounced and almost negligible in larger, deeper lakes ([11], [18], [34]). In such environments, the hydrodynamics associated with Winter II are much more important.

Winter II prevails in the late winter period, when snow cover melts and solar radiation is able to penetrate through the ice surface. The incoming radiation increases the temperature of the upper water column, leading to convective mixing directly beneath the ice

surface. As the warmed, heavier parcels of water sink, a convective mixed layer (CML) of approximately uniform temperature and density forms, which deepens in time [34]. The CML is separated from the ice by a thin, stable diffusive layer and lies above a quiescent layer which increases in temperature downwards toward the sediment [8]. Some studies consider a fourth, 'entrainment layer' between the CML and sediment layer [18], however, we ignore this level of detail in the present work. Radiatively driven convection dominates the circulation patterns of Winter II and continues until the mixed layer reaches the lake bottom, at which point spring overturn begins [64]. The corresponding visual for the second winter phase is shown in Figure 1.2, panel (b). Note that Winter I and Winter II can be of different durations depending on lake size or regional climate conditions.

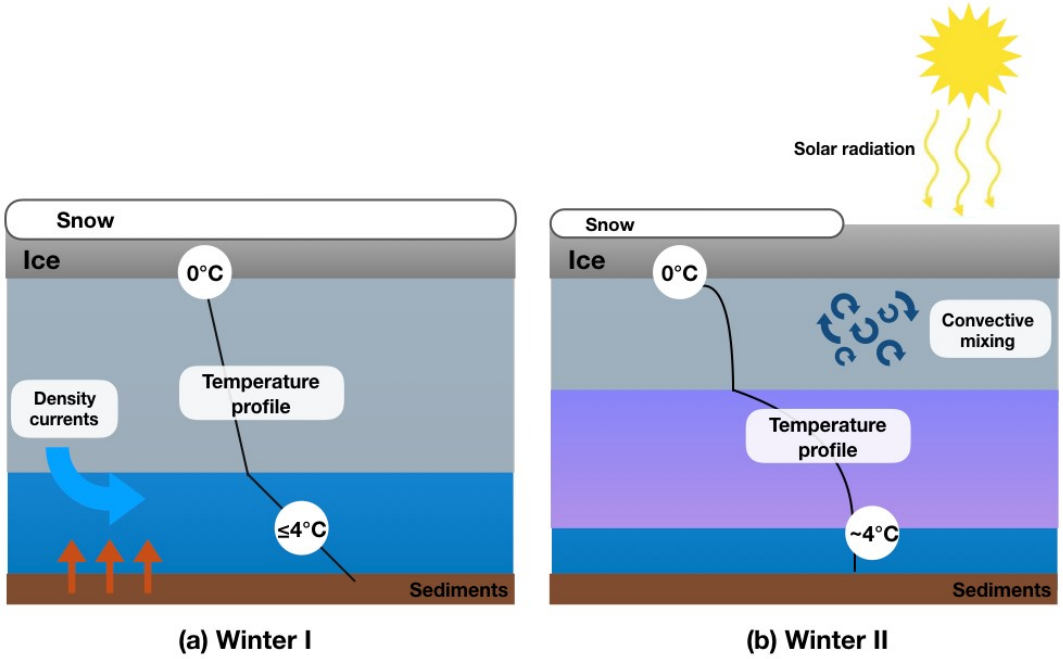

Figure 1.2: Depiction of the main physical processes and structure in ice-covered lakes in (a) early winter (Winter I), and (b) late winter (Winter II), following Kirillin et al. [34]. (a) Winter I hosts near total snow coverage, such that heat flux from the sediments drive density currents near the lake bed. (b) When the snow melts, solar radiation warms the upper water column, which drives a deepening convective layer in Winter II. The stratification pattern of Winter I develops shortly after ice-on and transitions to Winter II before ice-off. Colours represent the vertical temperature stratification, with a (a) two-layer, and (b) three-layer structure visible in Winter I and II, respectively.

Although able to generate gravitational instabilities under the ice surface in lakes, the solar radiation in winter is relatively weak [49]. Thus, the resulting convective mixing is also expected to be weak, which lends itself to explain why studies of radiatively driven convection in ice-covered lakes are quite sparse [8]. Similar to this, radiatively driven convective is a diurnally intermittent process, meaning instabilities are only actively generated during the day. However small the effects of solar radiation in late winter are on the underlying fluid dynamics, there still exist direct implications for primary producers. One example of such, is that increased light availability to the water column triggers photosynthetic activity [9]. Additionally, radiatively driven convection can regulate the distribution of nutrients throughout the water column, meanwhile working to suspend non-motile phytoplankton in regions with increased access to light for cell growth ([8], [33]). The mechanisms which cause mixing under the ice are well known and improved capabilities with sensors and new instruments have enabled extensive measurements of the thermal structure throughout the ice-covered period. However, many questions remain surrounding the physical processes of under-ice fluid dynamics given that little theoretical work has been done to provide any quantitative descriptions ([13], [42]).

1.4 Overview of Current Modelling

The primary requirement for a viable phytoplankton population to persist is a prolonged residence in the well-lit upper reaches of the water column. This alone allows phytoplankton to photosynthesize and build the tissue of the next generation ([47], [28]). Most taxonomic groups have a tendency to sink, including diatoms, and in general will not be able to sustain even a small portion of the population in regions with access to adequate light. Thus, the essential adaptation for phytoplankton is to increase the amount of time spent in regions with significant insolation by an appropriate mechanism. These mechanisms may span reduced sinking rates and flagella for controlled movement, however, they are meaningless unless the behaviour of the water column, and its associated motions (which tend to be much larger) are taken into account. If phytoplankton have a slow sinking velocity relative to their freshwater environment, they may be fully entrained. That is, despite the best efforts of the individual plankter, water movements are capable of either aiding or counteracting its intended course [47]. This is what current ecological models fail to emphasize, that at every scale, the water is never a passive component. If we are to consider under-ice processes, we must shift our focus to modelling the effects of radiatively driven convection on winter phytoplankton communities. An overview of current modelling, first focusing on ecological and then radiatively driven convection models, is presented below.

1.4.1 Ecological Models

Current ecological models fail to incorporate the majority of details of the hydrodynamics. Most popular appear to be 'reaction diffusion taxis' models, representing turbulence as a diffusion term that encapsulates fluid motion in an ad-hoc manner. Non-motile diatoms are at the mercy of movement within the water column: their distribution is dependent on either systematic currents or turbulent fluctuations and enhanced mixing to transport them to the photic zone. Given this, it seems odd that current ecological models have not accounted for fluid motion beyond simple parametrizations.

Huisman and Sommeijer [28] used a reaction-advection-diffusion model considering a stratified water column separated into two distinct layers to model phytoplankton growth. They were able to demonstrate that in addition to water column mixing, the depth of light penetration affects phytoplankton species composition. That is, the maximal sustainable sinking velocity is inversely proportional to the turbidity of the water column, meaning species are more liking to sink out of turbid waters as opposed to clearer ones. In a similar study predicting changes in species composition, Huisman et al. [29] developed a competition theory that predicts how shifts in turbulent mixing processes in the water column affect different phytoplankton species access to light. The predictions from the model were compared to and found consistent with a lake experiment that utilized artificial mixing. It is worth noting that neither of these studies consider under-ice processes nor do they properly account for the fluid dynamics.

Another study focusing on the interplay between phytoplankton, nutrients and light, uses numerical solutions of a similar one-dimensional reaction-diffusion-taxis model. Klausmeier and Litchman [35] assumed poorly mixed conditions in the water column, with passive movements due to turbulence modelled by eddy diffusion (holding the diffusion coefficient constant over depth). This model can be used to explain many patterns of algal distribution found in poorly mixed aquatic systems. Diehl [17] on the other hand, applies two variants of a dynamical model to understand better connections between mixing depth, nutrient supply, phytoplankton and light climate. This model applies the well known Beer-Lambert law to account for light intensity at a given depth, but it too constitutes an example of an ecological model that fails to properly account for fluid motions.

Note that each of these models focuses on the open-water column, consistent with the earlier point that the focus in the literature has been on the warmer summer and early autumnal months. Given that these models essentially ignore fluid mechanics, and furthermore, under-ice processes, it is no surprise they fail to mention the convective mechanisms at work within the water column. Hence, we shift our attention and consider these next.

1.4.2 Radiatively Driven Convection Models

As mentioned in the previous section, the vertical structure of the water column under the ice in late winter (early spring) is characterized by three layers: a thin, stable under-ice diffusive layer, followed by a convective mixed layer (CML), and finally a stably stratified quiescent layer below ([34], [58]). Many studies of radiatively driven convection in ice-covered lakes assume this structure exists *a priori*, and somewhat backwards, work to describe the associated processes in these layers. However, these descriptions do not often extend to physical fluid-processes, since the focus is on one-dimensional measurements and one-dimensional models most of the time. Radiatively driven convection in lakes is usually identified from time series temperature (or density) measurements ([45], [13]). This is due to the fact that convective motions driven by radiation, or in other words, the gravitational instabilities, are very weak so direct velocity measurements are challenging [63]. The convective mixed layer is often identified as the region where the the vertical temperature (or density) gradient is nearly zero, beginning immediately below the stable under-ice surface layer ([18], [43]).

Farmer [18] presented the first organized study of radiatively driven convection as it occurs in ice-covered lakes, specifically in Babine Lake, Canada. A one-dimensional, two layer model framed in terms of the mechanical energy budget was used to calculate the fraction of kinetic energy lost to viscous dissipation. The rate of dissipation of kinetic energy is commonly used to quantify the convective mixing efficiency [58], which has a significant effect on the growth of the mixed layer [18]. In fact, this paper is best known as providing the first description of a developing mixed layer based on large-scale observations.

In a more recent paper, Mironov et al. [43] provide a comprehensive review of past studies focused on solar-induced convective mixing. Similar to Farmer [18], they examine the vertical temperature structure and mixed layer deepening beneath ice-covered lakes, but with a larger focus, unspecific to any single temperate or polar lake. Their mixed layer model, which simulates deepening of the CML, is based on the turbulence kinetic energy (TKE) budget and a modified mixed layer scaling. The depth of the convective layer serves as an appropriate length scale, however, as opposed to employing the more commonly known Deardorff velocity scaling (based on the surface-buoyancy flux) they present a modified convective velocity scaling suitable for the case of volumetric radiative forcing. This new velocity scale, w_R, is a measure of kinetic energy of convective motions and depends on the optical properties of the water column; these affect how heating is distributed beneath the ice-surface. This scaling, which compared well with large-eddy simulations of turbulence kinetic energy (TKE), is the most notable contribution of this paper to the RDC literature. Although frequently cited, this paper focuses only on de-

scribing bulk properties of the flow under-ice and not the details of motion. Nevertheless, many studies have incorporated this scaling into their TKE budgets. One example of such is the paper of Jonas et al. [32], who investigated radiatively driven convection by means of a temperature microstructure technique to estimate the rate of energy dissipation in the water column.

The studies above are based on the analysis of the turbulent kinetic energy budget. Another avenue of research is the mechanical energy budget, where focus is on the energy pathway within a given system, for example, the under-ice environment in freshwater lakes. The temperature of the convective mixed layer has a complex dependence on how incoming radiative energy is vertically distributed. Mass and momentum budgets in the equations of fluid motion allow a simple derivation of the mechanical energy budget that involves the rate of change of the kinetic and potential energy. The potential energy can be further decomposed into a background and available component. Penetrative solar radiation increases both available and background potential energy, but only the former can drive fluid motions. That is to say, background potential energy cannot be converted to kinetic energy, but rather serves as an indicator of total heat content and homogenization of the temperature field by 'turbulent' mixing. The studies of Ulloa et al. [55] and Winters et al. [61] define both an evolution equation for the background and the available potential energy. Consistent with these authors, we stick to the inversely stratified regime and do not consider the effects of cabbeling which occurs with mixing near the temperature of maximum density.

The work of Ulloa et al. [55] examines the mechanical energy budget and the mixing efficiency of ice-covered, Boussinesq flows, with emphasis on the role of the radiative buoyancy flux (the primary forcing mechanism). Similarly, Winters et al. [61] derive and analyze the mechanical energy budget for shallow ice-covered lakes subject to penetrative solar radiation, focusing on the transformation of this radiation once it passes through the ice surface. The energy balance equation allows the authors to obtain an indirect estimate of the mixing efficiency for radiatively driven convection, which results in changes to the underlying stratification.

The mechanical energy budget as well as the turbulent kinetic energy budget have been given significant attention in the literature, both of which have their weaknesses and strengths. Mechanical energy budgets are derived from first principles and hence consider accurately the fluid dynamics, but they are not predictive. That is, they provide a way to analyze under-ice dynamics at a given time but cannot evolve those dynamics any further, providing only a limited view and subsequent understanding of the under-ice environment. At best, the turbulent kinetic energy budget can be thought of as an empirical one-dimensional model, ignorant of first principles, that is fit with parameters and

finally solved for some quantity (typically mixing efficiency and/or dissipation rate). Note that the turbulent kinetic energy budget is a reduction of the mechanical energy budget in that it only considers the fluctuating part of the velocity field. Their popularity and prominence in the literature is attributed to the fact that these models are, in general, easier to compare with field data than are numerical simulations. However, it is not clear that fully turbulent scaling theories actually apply under the ice, due to the low Reynolds number of flow therein (if we consider a length scale of 1 m and flows on the order of 1 mms^{-1}, a rough estimate gives $Re \approx 10^3$, indicative of transitional rather than turbulent flows). Essentially, the aforementioned studies apply these theories without considering that the associated scalings might not be the best, or even correct, measurements in this regime. In the winter, solar radiation is relatively weak [49], implying that convective mixing driven by this heating should also be weak. Turbulent phenomenon should not be sought to explain under-ice processes if it has not been shown that the under-ice environment is truly turbulent; this is something that has yet to be quantified. Given the issues surrounding winter time sampling and the difficulty of under-ice measurements, the easiest way to do this is through simulations. Although simulations may not properly account for some wind motions or radiative heating, making them less comparable to field data, they do properly account for the fluid motions; an impressive and necessary achievement to heighten our understanding of under-ice processes. Hence, it is important to consider studies that focus on two-dimensional or even three-dimensional dynamics.

The role of lateral flows in the energy and heat balance of radiatively driven under-ice convection is the focus of the more recent study of Ulloa et al. [56]. Sloping boundaries in the littoral zone correspond to shallower regions in the lake basin. These are differentially heated to warmer temperatures, driving gravity currents that transport warmed water down-slope into the deeper, pelagic zone. Using two-dimensional numerical simulations, the authors correctly resolve the associated hydrodynamics in the under-ice water column, ultimately concluding that advective fluxes due to differential heating contribute to the development of the mixed layer. Most often, mixed-layer dynamics are modelled and subsequently understood as one dimensional (vertical) processes ([43], [18]). Ulloa et al. [56] used a heat balance to show that neglecting these horizontal variations (due to gravity currents) will always underestimate the rate of mixed layer warming, assuming the lake morphology includes shallower zones. Hence, an explicit correction to the one-dimensional mixed-layer heat balance should be employed to correctly account for heating due to lateral processes.

Note that Ulloa et al. [56] consider convection in the mixed layer, as well as lateral gravity currents, both of which are driven by radiative heating under-ice. This thesis includes only the former, and without time-dependant radiative forcing as is considered

here. However, what the present research lacks in breadth and scale, it makes up for in the resolution of the under-ice hydrodynamics as well as investigating the associated implications of these water motions to primary producers. In fact, this seems to be the most common pitfall in the literature: either the hydrodynamics are properly discussed as in [56], or the study comments on interesting biological implications of under-ice flows without actually considering (quantifying) their effects. We will look at a few instances of the latter as they occur in the literature next.

The work of Forrest et al. [19] presents field observations of the thermal structure formed by penetrative convection in a mid-sized, temperate lake during the winter. Conductivity–temperature–depth profiles revealed convective plumes driving overturning within the surface waters. The paper makes use of a simplified velocity scaling to calculate the convective velocity of these gravitational instabilities. Similarly, the authors provide a calculation to determine how long it takes for frictional damping to dissipate generated kinetic energy during nightfall, given that radiatively driven convection is diurnally intermittent. The author's note that physical transport processes directly influence biological processes and indicate the need to link these two together to better understand freshwater ecosystems.

In this next paper, the importance of convective mixing is discussed in relation to the distribution of phytoplankton (and nutrients) throughout the water column. Matthews and Heaney [42] construct a pair of simple mathematical models to describe the influence of radiative heating on under-ice convective mixing in freshwater lakes. Both models solve the one-dimensional heat equation, assuming the water column is at rest, where the second model is an improvement over the first only in the fact that it considers an arbitrary number of layers, each given an initial temperature. It is important to note that neither of these computational models solve the Naiver-Stokes equations, but rather were applied to specific ice-covered lakes where the necessary physical data was available for a full analysis. The authors attempt to estimate the scale of vertical velocities of the water movements, as it pertains to phytoplankton production and species composition. Their estimate is based on the '1/3 power law' of a fully turbulent convective layer [42], derived from dimensional analysis and further supported by experiment.

With focus on Lake Onego (Russia), Bouffard et al. [9] investigated radiatively driven under-ice convection in three consecutive later winter periods (i.e. the CML was already well-developed), where direct solar forcing and changes in thermal structure of the water column were considered the most important observable parameters to characterize under-ice convection. Analytical scaling estimates of the convective velocity of the water column (responsible for entraining phytoplankton) were compared to in situ observations. Using this convective velocity, and other easily measurable parameters, they present a simple model for diatom growth employing a typical range of sinking speeds to evaluate how

radiatively driven under-ice convection affects non-motile phytoplankton. A winter field campaign conducted by Suarez et al. [52], also in Lake Onego, investigated the significance of diurnal patterns of convection to phytoplankton development. Although this paper does not present any models of phytoplankton growth, similar to Bouffard et al. [9], they were able to conclude that the vertical distribution of heat in the water column (which varies throughout the day) is important to quantify the effects that radiatively driven convection has on primary producers, especially in turbid lakes.

Perhaps the most useful comparison for the purpose of this thesis is the theoretical study of Kelley [33], who examined under-ice convective flow fields, determining which of these were able to suspend algae in the well lit upper reaches of the water column. Although less recent, this study achieved what most others have not, a balance between correctly accounting for fluid motions (beyond simple scalings, though these are employed) and considering their effects on phytoplankton communities. For a given flow field, a measure of suspension efficiency can be defined, this being the central concept of the paper. The author shows that the suspension efficiency of algal cells is dependant on the ratio of the sinking speed of the phytoplankton species, to the convective updraft speed of the water column. The convective updraft speed is related to both the depth of the mixed-layer as well as the solar insolation passing through the ice cover and is determined via scaling relationships (based on dimensional analysis and empirical studies). Note that the diurnal variation of convectively driven radiation reduces the suspension efficiency at night [33].

Many sources note that convective motions can suspend algal cells that sink slower than convective updrafts rise ([47], [28]), however, the approach of Kelley [33] correctly accounts for the associated hydrodynamics, a feature rare in the literature. Note that the details associated with convective mechanisms are often overlooked, largely because their description is governed by non-linear equations whose solution is quite difficult. The presentation by Kelley [33] is rather simplified, considering an example of a steady circulation flow field with 2-D geometry, but nonetheless an impressive addition towards improving our understanding of biological-physical interactions under ice. The components of the velocity field (see Equation 9 in [33]) are determined by the spatial derivatives of the circulation stream function, and provide a reasonable description of a convective eddy associated with (relatively) weak solar forcing. A small modification to the vertical velocity, w, allows for the consideration of the trajectory of algal cells heavier than water. The updated Equation 10 in [33] reflects this small, but important change. Essentially, the analysis of Kelley [33] applies tractable techniques of fluid mechanics (analytical mathematics), with an assumed trajectory for the motion of the convection, specifically, circular motion (see his Figure 1 [33]). However, he presents this figure and the subsequent stream function without justification that the convection under the ice is actually akin to the model of Langmuir

circulation. Additionally, Kelley [33] notes that his analysis, or one similar in character, could be accomplished via numerical simulation using the Navier-Stokes equations. In this thesis, we intend to do just that, with no *a-priori* assumption of the characteristic flow field associated with under-ice radiatively driven convection.

The present work is concerned with the hydrodynamics of cold water lakes and the implications of winter ice cover to underlying phytoplankton communities. To discern what is happening at the planktonic scale, we require high resolution. Using a non-hydrostatic, pseudospectral model, coined SPINS, we model under-ice fluid dynamics driven by incoming solar radiation in an idealized, rectangular domain. We refrain from modelling large-scale lake circulation given the relatively quiet nature of the under-ice environment. Several simulations are explored, altering one parameter at a time for the purpose of easy comparison. The equations of motion that are solved are the incompressible Navier–Stokes equations under the Boussinesq approximation subject to external (radiative) forcing. Employing direct numerical simulations (DNS), SPINS is able to resolve all the dynamics of interest.

Note that the absorption of incoming solar radiation throughout the water column is dependant on a number of factors, many of which are rapidly changing given the current climate crisis. For example, lakes with high proportions of dissolved organic matter (DOM) can be associated with murky, brown-coloured waters, depending on local relationships (more on this in the Background section ahead). These lakes would absorb radiation more effectively near the lake surface than say, clear, and relatively pristine waters. The distribution of solar radiation across the top of the water column drives convective motions that work to push phytoplankton out of the photic zone; this is the region of the water column that harbors sufficient light conditions for photosynthesis and growth. The goal of this work is to determine how variations in the absorption of incoming solar radiation affect the distribution of phytoplankton beneath the ice surface. To do this, we must quantify the effects of radiatively driven convection in two lakes which experience similar winter characteristics, but differ in their under-ice optical environments.

To the best of my knowledge, the analysis of under-ice radiatively driven convection via direct numerical simulations (DNS) has yet to be explored. A recent study of sub-glacial lakes by Couston [15] used two-dimensional direct numerical simulations to investigate the characteristic temperature fluctuations and velocities experienced in these freshwater environments. However, the unique forcing mechanism in this case is geothermal heating rather than radiative heating because unlike ice-covered lakes, sub-glacial lakes typically have much thicker ice cover and hence are not influenced significantly by solar radiation. Combined with the fact that these environments are unlikely to host appreciable winter algal blooms, the proposed model is significantly different than anything currently pre-

sented in the literature. Furthermore, the associated convective motions in the under-ice environment are weak such that the literature on convection driven by surface fluxes (as occurs in the atmosphere) is not relevant for comparison to the current work.

1.5 Outline of Thesis

The format of this thesis is as follows. Chapter two provides the relevant background necessary to understand the proposed model and subsequently discusses the numerical methods used. It begins with an in-depth overview of lake optics focusing on properties that alter the absorption and attenuation of light through the under-ice water column. One of these properties is the amount of coloured dissolved organic matter (CDOM) in the water column. Thus, we present and discuss two sites, namely Lake Erie and Lake Onego, which share enough winter traits to allow for an easy comparison throughout this work, but differ in their concentration of coloured dissolved organic matter. The assumptions underlying the Boussinesq approximation are outlined to provide context for the governing equations used in the model. Finally, the numerical methods used and any underlying model assumptions, including relevant diagnostic quantities are presented. Chapter three outlines the results of the four cases as defined in the previous chapter. The cases consider variations to lake thermal structure, incoming (under-ice) radiation, and associated time-scales (day versus day night). Each case considers Lake Erie and Lake Onego in turn, save for the first presentation (the case without stratification), which focuses only on Lake Erie. These parameters were varied to identify changes in physical and subsequently, biological processes occurring within the water column. The discussion focuses on these coupled bio-physical lake processes and makes comparisons to relevant measurements quoted in the RDC literature whenever possible. The fourth and final chapter discusses the primary conclusions and identifies directions for future work.

Chapter 2

Background and Methods

2.1 Lake Clarity and Light Attenuation

2.1.1 Absorption and Attenuation of Light (Effects of CDOM)

The absorption and attenuation of light by the water column are major factors controlling both lake warming, which directly influences thermal stratification patterns, as well as potential photosynthesis ([59], [27]). Solar radiation is received at the Earth's surface in two forms: (i) as direct radiation from the Sun, and (ii) as diffuse radiation from the sky due to scattering in the atmosphere. To obtain the amount of incoming radiation at an ice-covered lake surface, for example, one must consider the concept of irradiance; that is, the transfer of radiative energy from the Sun/atmosphere (considering contributions over all directions) into the lake itself [38]. The intensity of solar radiation reaching an ice-covered lake gradually decreases with depth throughout both the ice cover and the water column below. This relates to the concept of spectral attenuation, which is the gradual loss of flux intensity through a medium due to the absorption or scattering of light. Two spectral quantities with direct relevance to ice-covered lakes are reflectance and transmittance. Reflectance is defined as the ratio of outgoing to incoming solar radiation. In some instances, the reflectance is simply referred to as the surface albedo [9]. Transmittance on the other hand, can be defined as the ratio of radiation directly beneath the ice surface to the incoming solar radiation above. Hence, how much light is transmitted is directly related to how much light is reflected. In this thesis, the amount of radiation entering the water column beneath the ice surface will be the most important parameter.

Ice and snow cover act as a filter with respect to the amount of solar radiation that is able to penetrate through the lower boundary of the ice surface and into the water column below. In other words, an ice-covered lake with an overlying blanket of snow is associated with high reflectance, or increased albedo. In winter, most boreal lakes are covered by congelation ice, which has approximately the same effect on light penetration as does a liquid water layer of the same depth [34]. While the albedo depends on both the thickness and type of ice cover, it is most significantly increased by snowfall [46], with values approaching as high as 0.9 dependant on the snow-type (wet versus dry, where dry, fine-grained snow is most reflective [34]). This means that 90% of incoming solar radiation would be reflected from a snow-covered surface, leaving little to penetrate into the waters below. Dependant upon regional weather conditions, the albedo can increase, decrease, or remain the same, with drastic changes commonly observed on short time scales [6]. In early spring, as the snow-ice cover begins to melt, the transparency increases and subsequently, the light levels beneath the ice surface do as well. The deeper light penetrates into the water column, the deeper that photosynthesis can occur. The maximum depth at which phytoplankton can sustain a viable population is determined by light levels. The photic zone (sometimes euphotic zone) is delineated by the depth at which the amount of light available is reduced to 1% of the surface level ([27], [34]). Under ice and potentially snow cover, the definition of the photic zone needs to be modified to take into account the reflectance and transmittance of the ice surface.

To summarize what we have discussed, the parametrization of the transfer of solar energy through ice-covered lakes can be broken into three steps: (i) depending on properties of the snow and ice cover, a significant portion of the incoming solar radiation is reflected, (ii) the portion that evades reflection is partially absorbed throughout the ice-snow layer, and finally, (iii) what is left of the solar radiation past this point is absorbed throughout the water column [34]. The vertical distribution of light in the ice-snow layer as well as the water column is dependant on a number of factors. For example, the rate at which light decreases with depth in the water column largely depends upon the amount of light absorbing substances (mostly organic carbon compounds washed in from the watershed), whereas in the case of ice and snow, the amount of scattering caused by suspended materials, or air pockets, is most prominent. The fraction of incoming solar radiation absorbed or scattered over a one meter thickness of material is known as the vertical attenuation (extinction) coefficient, k (units: m^{-1}) [27]. For the purpose of this discussion, said material could be either snow, ice, or the water column under their cover. In this thesis, we will only consider an attenuation coefficient for the water column and will reflect absorption/attenuation through the snow-ice layers as a reduction in the solar radiation at the ice-water interface.

In lakes with low k-values, light is able to penetrate deeper into the water column than is possible in those with higher k-values. A lake's associated k-value provides an indication of the turbidity of the water column; higher attenuation coefficients are often linked with turbid waters, whereas lower values hint at relatively clear waters [27]. What this means, is that different lakes are subject to different optical properties since attenuation coefficients vary depending on the concentration of organic (biotic) and inorganic (abiotic) constituents within the water column ([42], [30]). Further to this, for both ice and water, the attenuation coefficients depend on wavelength. As mentioned previously, we only consider an attenuation coefficient for the water column in this work. A wavelength dependant attenuation coefficient implies that absorption is not uniform over wavelengths. For example, as the value of the attenuation coefficient increases, the absorption of light at lower wavelengths (blue spectral components) increases more rapidly than at higher wavelengths (red spectral components). An explanation for this phenomena stems from the fact that dissolved organic materials and phytoplankton residing in the water column have preferential absorption of light at lower wavelengths ([30], [9]).

Characterization of the Light Environment

Physical processes occurring under ice-covered lakes are critically dependant on the vertical distribution of downward irradiance, and as such, most mechanistic freshwater models consider the attenuation of light throughout the water column [59]. Most often, to determine the vertical distribution of downward irradiance, $I(z)$, at a depth, z, the incident irradiance, I_0, is assumed to be attenuated according to the Beer-Lambert law [38]

$$I(z) = I_0 \exp(-z/\xi_1) \tag{2.1}$$

where ξ_1, the attenuation length (reciprocal of the attenuation coefficient, units: m), is assumed constant with depth. This assumption implies that the water column is optically homogeneous, and furthermore that light can be treated as a monochromatic source (independent of wavelength) ([51], [9]). Note that I_0 represents under-ice irradiance, meaning that reflectance/transmittance (albedo) effects of the overlying ice surface and snow cover have been taken into account. Essentially, the Beer-Lambert law describes the decrease of incoming solar irradiance with depth.

The assumptions made by light attenuation models directly affect the thermal structure of the water column which has further implications for primary producers. Spectral properties are wavelength dependant, so to assume that the water column is optically homogeneous is perhaps the easiest, but not the most accurate approximation. To improve

upon the Beer-Lambert model, one may consider the spectral decomposition of downward irradiance divided into many wavelength bands [51]

$$I(z) = I_0 \sum_{i=1}^{n} a_i \exp(-z/\xi_i) \tag{2.2}$$

where n represents the number of these wavelength bands. Increasingly complex models employ higher values for n, and similar to before, ξ_i represents the attenuation length, only now the subscript i indicates wavelength dependency. The irradiance constant, a_i, weights the approximate influence of each band. Although the spectral decomposition into many wavelength bands potentially requires that many degrees of freedom be specified, this level of complexity may need to be pursued for wavelength-dependant processes, such as photosynthesis [51].

To accurately characterize the under-ice light environment as it pertains to phytoplankton populations, the light intensity or more specifically, the photosynthetically active radiation beneath the ice-surface should be considered. Photosynthetically active radiation (PAR) is the amount of radiation available for photosynthesis and hence, the survival of freshwater phytoplankton, that spans over the spectral region from 400 to 700 nm ([7], [45], [30]). In some instances, this range of wavelengths may be referred to as the visible spectrum, depending on the context in which it is considered. Incoming solar radiation can be fractionated by wavelength, where PAR represents 45-50%, ultra-violet (UV) radiation approximately accounts for 5%, and the longer wavelengths (>700 nm) make up the difference [45]. Longer wavelengths attenuate more rapidly through ice and snow such that it is often assumed that only PAR and UV radiation contribute to the under-ice irradiance, I_0. Often, even UV radiation is neglected given the relatively small contribution of energy contained in this region as compared to that in the PAR spectrum ([10], [37]); this is the assumption we will adopt in this work.

Effects of Coloured Dissolved Organic Matter (CDOM)

Dissolved organic matter (DOM) alters lake warming trends in that it strongly attenuates light by absorbing PAR in the surface waters of lakes; this strong attenuation increases the temperature of the upper water column and restricts the depth of the photic zone as well as the depth through which nutrients are mixed (deeper layers are effectively cut off) [16]. Recall from the Introduction that dissolved organic matter (DOM) constitutes the largest organic carbon pool in the water column ([65], [25]) and is frequently used as an indicator of climate change. Dissolved organic matter in lakes originates from the surrounding

catchment, meaning it is terrestrial in origin (allochthonous DOM), however, it may also be produced within the lake itself as a result of biological activity (autochthonous DOM) ([16], [20]). The light absorbing coloured (or chromophoric) fraction of DOM is known as coloured dissolved organic matter (CDOM) [48]. Often CDOM in lake waters is positively correlated with the bulk pool of dissolved organic carbon (DOC), although this relationship is local and may change from region to region ([25], [48]). DOC refers specifically to the carbon in DOM, and hence the two terms will be used interchangeably in this thesis with preference given to the broader classification of DOM. Recent climate change predictions for boreal regions reveal that increased loads of organic matter (DOM/DOC and CDOM) will be deposited into lake waters as a result of altered hyrdological patterns (increased precipitation) ([25], [41]). This increase of organic content leads to adverse water quality conditions, including water color change (brownification) and increased light attenuation of shorter wavelengths. Photosynthesis depends fundamentally on light, meaning that changes in light penetration and lake transparency will have dire consequences for phytoplankton [27].

In models of primary production, a common simplification is to aggregate across the wavelengths of photosynthetically active radiation and define a single attenuation coefficient, k_{PAR}, ([9]) which allows use of the Beer-Lambert law [59] (see Equation 2.1). As discussed earlier, the use of a single attenuation coefficient for incoming solar radiation is not strictly valid. Most concerning is this simplification as applied to CDOM rich waters, where the attenuation of PAR across wavelengths differs greatly; short wavelength radiation is strongly absorbed as compared to the rest of the visible spectra [10] with this absorption declining exponentially with increasing wavelength (see Bouffard et al. [9] Figure 5 (a)). Effectively, this means that only the largest wavelengths will still contain energy, and thus contribute to the heat flux, at greater depths. High CDOM absorption limits light penetration in the water column (see Figure 2.1), thereby reducing the depth of the photic zone. Further to this, the quantity and quality of PAR is diminished in CDOM-rich waters with correlated consequences for phytoplankton growth (their ability to photosynthesize is effectively reduced) [25]. Many ice-covered lakes, especially those at high latitudes, are CDOM-dominated and climate change will only serve to increase this total ([9], [20], [16]). The presence of CDOM modifies the spectral distribution compared to PAR based light absorption, and hence, a more complex parametrization of irradiance (such as Equation 2.2) should be employed to accurately quantify radiatively driven under-ice convection in high CDOM lakes.

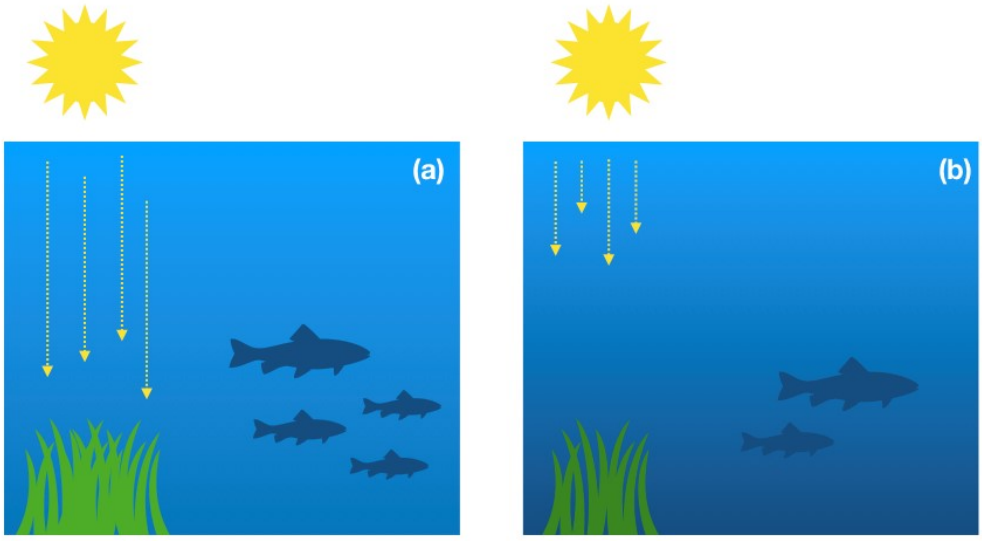

Figure 2.1: Schematic depicting changes in light penetration between (a) a relatively clear lake and (b) a CDOM-dominated water column, with increased turbidity. Note that the depth of the photic zone is significantly decreased by the presence of dissolved organic matter limiting biological activity (fish, plant growth) at greater depths.

2.1.2 Site Description (Lake Erie vs. Lake Onego)

In this thesis, we consider two different lakes to compare and contrast the effects of increased CDOM levels on light attenuation and subsequently, under-ice radiatively driven convection. The difference in CDOM concentrations is reflected by differing attenuation coefficients (lengths) in our model. The lakes under investigation have been chosen due to shared winter traits and recent prominence in the literature. An example of these similarities is that both lakes contain winter diatom blooms of the same species and maintain significant ice cover throughout the season. The first lake we consider, Lake Erie (Canada), has moderate CDOM levels whereas Lake Onego (Russia) boasts moderate to high levels. Recent research indicates that CDOM levels are on the rise in Lake Erie as an effect of climate change. Hence, we consider Lake Onego to provide a glimpse into the possible effects of increased attenuation coefficients on radiatively driven under-ice convection and the implications for winter phytoplankton blooms in Lake Erie. In this work, we assume significantly higher concentrations of coloured dissolved organic matter in Lake Onego to contrast clearly between the two environments. We describe briefly each 'site' below, providing further details of the information summarized here.

The Laurentian Great Lakes, located in North America, contain nearly 20% of all surface freshwater on Earth [65]. Lake Erie is the smallest of the Great Lakes by volume (480 km^3) and is classified as a large, shallow lake (mean depth of 19 m) based on measurements of width, length, and depth ([26], [59]). The shallow depth of Lake Erie explains why near total ice cover occurs most winters. Under this ice cover, the presence of diatoms (specifically, *Aulacoseira islandica*) has been frequently observed [54]. The lake commonly experiences a weak, inverse stratification with water temperatures less than the temperature of maximum density ($T_{md} \approx 4°C$). Weak in this sense implies that the water column beneath the ice is nearly isothermal (at a constant temperature) and this is hypothesized to occur due to wind-induced mixing beneath the water column allowed by leads, or gaps in the ice [54]. Further to this, Lake Erie has a moderate concentration of CDOM in each of its three basins, where CDOM measurements in winter are consistently higher than those across the lake in summer. Light extinction coefficients of PAR obtained by Twiss et al. [54] suggest that the under-ice water column fosters a shallow photic zone.

Recently, the Great Lakes have undergone significant ecological and environmental changes related to the current climate crisis. Being the southernmost lake of the interconnected system, Lake Erie is influenced by the upstream Great Lakes in addition to local inputs, such as those from rivers or streams; both of these influences contribute to higher concentrations of allochthonous DOM (terrestrially-derived organic matter) in the lake water body [65]. In addition to this, the Lake Erie watershed supports about one-third of the population of the Great Lakes region [65], making it further susceptible to fluctuations of allochthonous DOM. Consistent with these trends, it has been found that DOM concentrations have increased in Lake Erie over time ([65], [41]). Further to this, the local relationship between DOM and CDOM in Lake Erie is positively correlated [14], meaning that CDOM concentrations are increasing as well. It is for this reason that we consider Lake Onego as a proxy for future changes in physical (and biological) under-ice processes.

Lake Onego (sometimes Lake Onega [9]), located in Karelia (Russia), is the second largest lake in Europe with a surface area of 9700 km^2 ([52], [62]). Ice cover prevails for several months each winter, however, over the last 60 years ice cover duration has decreased by approximately 20 days per year [62]. Nevertheless, the diatom species *Aulacoseira islandica* remains dominant in Lake Onego during the winter months [52]. The dark colour of Lake Onego alongside the large absorption observed over short wavelengths in several studies ([9], [52]) indicates that a large fraction of DOM behaves as CDOM. In fact, Lake Onego has moderate to high coloured dissolved organic matter, meaning negative effects on phytoplankton development will be more pronounced in this environment when compared to Lake Erie. We will comment further on this in the Results and Discussion section below.

2.2 The Boussinesq Approximation

The Boussinesq approximation finds wide use in the published literature on environmental fluid mechanics as it performs remarkably well in the vast majority of naturally occurring cases. In this thesis, we make use of the Boussinesq approximation in which density changes in the fluid may be neglected in both the continuity and momentum equations, except for in the gravity, or buoyancy, term. Furthermore, this approximation treats the properties of the fluid (physical parameters) as constants. Although the particular derivations associated with the Boussinesq approximation are not important to the results of this thesis, we will discuss some of the main points below, paying particular attention to the equations involved (2.4, 2.10, 2.11) and the underlying assumptions validating their use.

Continuity Equation

The continuity equation (conservation of mass) in its most general form can be written as

$$\frac{1}{\rho}\frac{D\rho}{Dt} + \nabla \cdot \vec{u} = 0 \tag{2.3}$$

where ρ is the fluid density, $\frac{D}{Dt} = \frac{\partial}{\partial t} + \vec{u} \cdot \nabla$ is the material derivative, and $\vec{u} = (u, v, w)$ is the fluid velocity. The first term represents the rate of change of density following a fluid particle whereas the second term accounts for changes in volume. The Boussinesq approximation replaces Equation 2.3 by the incompressible form (see discussion below), namely,

$$\nabla \cdot \vec{u} = 0 \tag{2.4}$$

with approximate equality being understood. It is important to note that the Boussinesq approximation does not regard the density as a constant along the direction of motion, rather, it assumes that the magnitude of the first term in Equation 2.3 is small in comparison to the velocity gradients [36]. Thus, Equation 2.4 holds irrespective of whether the flow is steady or not, with the additional requirement that density changes within the fluid must be small with respect to the reference density and that fluid velocities are much less than the speed of sound within the medium of context. The latter restriction can be understood in terms of a condition on the Mach number of the flow, U/c, where U is a characteristic flow speed and c is the speed of sound in the medium ($c = 1470\text{ms}^{-1}$ for water [36]). The Mach number must be less than 0.3 for the validity of the Boussinesq approximation. In liquids, the incompressibility assumption is quite good since flow speeds are typically much less than the speed of sound in water ($U \ll c$). The Boussinesq approximation effectively

filters sound (compression) waves from the equations. However, in this work, we are not concerned with sound waves and the assumption that such waves effectively propagate at infinite speed is acceptable [36].

The final restriction of the Boussinesq approximation is that density changes are due to temperature variations (or salinity in relevant cases, though such effects are ignored in this thesis) but never pressure [36]. That is, if the vertical scale of the flow is so large that hydrostatic pressure variations can cause large changes in density, then compressibility effects become important. For example, the pressure dependence of the density might be expected to apply in a very deep lake (e.g. Lake Baikal). The vertical extent of the domain considered in this thesis is quite small, and realistically, does not represent the appropriate depth of either lake in question. Nevertheless, the small vertical scale encountered ensures that this last condition is met. Note that if the compressibility effects are small such that the density changes are in fact caused by temperature changes alone, for the Boussinesq approximation to apply, the temperature variations in the flow must be small as well. With an understanding of the assumptions behind the Boussinesq approximation in hand, the remaining conservation of momentum and thermal energy (heat) equation can be simplified.

Momentum Equation

Given the incompressibility condition (introduced by Equation 2.4) the momentum equation reduces to that seen in the Navier-Stokes equations for the case of constant density [36]

$$\rho \frac{D\vec{u}}{Dt} = -\nabla p + \rho g \hat{k} + \mu \nabla^2 \vec{u}. \tag{2.5}$$

Consider next a hypothetical background state in which the fluid is stationary ($\vec{u} = 0$), the density everywhere is ρ_0, and the pressure varies only in vertical as $p_0(z)$. With this in mind, Equation 2.5 reduces as follows:

$$\nabla p_0 = \rho_0 \vec{g} \quad \text{or} \quad \frac{dp_0}{dz} = -\rho_0 g \hat{k} \tag{2.6}$$

where in the second line we have have made note of the fact that $\vec{g} = -g\hat{k}$. Equation 2.6 implies that the background state is in hydrostatic balance. For the density field to induce any motion, there must be an added perturbation, $\rho(x, y, z, t)$. Hence we write,

$$\rho = \rho_0 + \rho'(x, y, z, t) \tag{2.7}$$

with a similar decomposition assumed for the pressure, p,

$$p = p_0 + p'(x, y, z, t). \tag{2.8}$$

Using the above decomposition of density and pressure in Equation 2.5 and noting that we can use Equation 2.6 to simplify, we arrive at the following,

$$\left(1+\frac{\rho'}{\rho_0}\right)\frac{D\vec{u}}{Dt} = -\frac{1}{\rho_0}\nabla p' + \frac{\rho'}{\rho_0}g\hat{k} + \nu\nabla^2\vec{u} \tag{2.9}$$

where we have divided the entire expression by a common factor of ρ_0. In this equation, ν is the kinematic viscosity, defined as μ/ρ_0 (units: $\mathrm{m^2 s^{-1}}$), where μ represents the dynamic viscosity. The density variations only contribute a small correction to the inertia term on the left hand side ($1 \gg \rho'/\rho_0$). Hence, density changes in the fluid may be neglected except for in the gravity (buoyancy) term where their effects become important. In this thesis, the density differences in the buoyancy term are responsible for driving convective motions when the upper layer of the water column is heated by incoming solar radiation.

Thus, the equation for conservation of momentum for a Boussinesq fluid (dropping primes for notational convenience) is given by

$$\frac{D\vec{u}}{Dt} = -\frac{1}{\rho_0}\nabla p + \frac{\rho(T)}{\rho_0}g\hat{k} + \nu\nabla^2\vec{u} \tag{2.10}$$

where we note that the changes in density are related to differences in temperatures via an equation of state, $\rho(T)$. Note that the equation of state considered is problem specific, although a linear dependence of density on temperature is common. In such flows with temperature variations, we need an additional equation to describe in full the dynamics; this is provided by the heat equation, which we discuss next.

Heat Equation

The last conservation law that is simplified using the Boussinesq approximation is the heat equation (derived from the first law of thermodynamics). Rather than dive into the details of the derivation, we refer the reader to resources external to this thesis such as Kundu [36]. Here we quote the simplified equation, noting that the effects of heating due to viscous dissipation are ignored

$$\rho C_p \frac{DT}{Dt} = -\nabla\cdot\vec{q}. \tag{2.11}$$

Commonly the heat flux is assumed to follow the Fourier diffusion law ($\vec{q} = -k\nabla T$) in which case Equation 2.11 simplifies to

$$\frac{DT}{Dt} = \kappa\nabla^2 T. \tag{2.12}$$

The constant $\kappa = k/\rho C_p$ is known as the thermal diffusivity (units: $\mathrm{m^2 s^{-1}}$), where C_p as occurs in the denominator is the specific heat capacity at constant pressure. Note that any terms associated with external forcing, contributing to the overall heat flux, $\vec{q}$, would appear on the right hand side of Equation 2.11.

2.3 Governing Equations and Numerical Methods

In the context of early spring-time, temperate lakes, the stratified Navier-Stokes equations under the Boussinesq approximation are the relevant set of governing equations. However, most literature on simulating lakes make at least some simplifications (commonly, the hydrostatic assumption). We will retain the full (non-hydrostatic) equations since we will consider a very small portion of a lake under ice cover. In our context, temperature differences in the domain are small (typically less than 0.1 degrees centigrade), implying that density differences will be extremely small as well. The governing equations under the Boussinesq approximation with reference density, ρ_0 ($\rho_0 = 1000$ $\mathrm{kgm^{-3}}$), read:

$$\nabla \cdot \vec{u} = 0, \tag{2.13}$$

$$\frac{D\vec{u}}{Dt} = -\frac{1}{\rho_0}\nabla p - \frac{\rho(T)}{\rho_0} g\hat{k} + \nu\nabla^2\vec{u}, \tag{2.14}$$

$$\frac{DT}{Dt} = \kappa\nabla^2 T - \frac{1}{\rho_0 C_p}\left(\frac{\partial I(z)}{\partial z}\right), \tag{2.15}$$

$$\frac{DP}{Dt} = \kappa\nabla^2 P \tag{2.16}$$

where $\frac{D}{Dt}$ is the material derivative, $\vec{u} = (u, v, w)$ is the fluid velocity, p is the pressure, ρ is the density, ν is the kinematic viscosity ($\nu = 10^{-6}$ $\mathrm{m^2 s^{-1}}$), g is the acceleration due to gravity ($g = 9.81$ $\mathrm{ms^{-2}}$), κ is the thermal diffusivity ($\kappa = 10^{-7}$ $\mathrm{m^2 s^{-1}}$), C_p is the specific heat capacity of water at constant pressure ($C_p = 4180$ $\mathrm{Jkg^{-1}\ K^{-1}}$), T is the temperature, and P represents the concentration of phytoplankton within the water column. Note that the concentration of phytoplankton is modelled as a passive tracer and will commonly be referred to as a dye in this thesis; this is to remind the reader that diatoms are non-motile and that growth and population dynamics are ignored (more on this later). We assume that the thermal diffusivity constant, κ, holds for Equation 2.16 as well. Since the stratification is temperature controlled, the Prandtl number ($Pr = \nu/\kappa$) is held fixed at $Pr = 10$. Here $\rho(T)$ (as appears in the second term on the right hand side of Equation 2.14) is the seven-term polynomial equation of state specified according to Brydon [12].

The second term on the right hand side of the heat equation (2.15) deserves further comment. In this thesis, the heat flux is assumed to follow the Fourier diffusion law but because we consider an external heat flux (downward radiative forcing), we must add an additional argument. Hence, $\vec{q} = -k\nabla T + I(z)\hat{k}$, where the function $I(z)$ represents the downward radiative forcing divided into three wavelength bands across the PAR spectrum (see Table 2.1 and 2.2 for appropriate constants)

$$I(z) = I_0 \left[R_1 \exp\left(\frac{z - L_z}{\xi_1}\right) + R_2 \exp\left(\frac{z - L_z}{\xi_2}\right) + R_3 \exp\left(\frac{z - L_z}{\xi_3}\right) \right]. \tag{2.17}$$

Here I_0 represents under-ice irradiance, meaning that reflectance/transmittance (albedo) effects of the overlying ice surface and snow cover have been taken into account. As mentioned above, it is assumed that only PAR radiation contributes to the under-ice irradiance. Values for I_0 are outlined in Table 2.2, and represent conditions typical of late/winter early spring, with the assumption of moderately high albedo [9]. The irradiance constants, (R_1, R_2, R_3), are analogous to a_i in Equation 2.2 and sum to one. The values associated with the set were chosen using Jerome et al. [30] as a guide (see their Figure 2), where we assumed that the weight associated with each band was approximately equivalent, $R_1 = R_2 = R_3 \approx 0.33$. We employ Okham's razor and claim that this is a reasonable simplification given the paucity of measured values available in the literature. Recall that the attenuation of light across wavelengths is not constant and differs greatly in CDOM rich waters specifically. This motivates our use of three bands rather than modelling incoming radiation as a monochromatic source since we consider two lakes, both of which have at least moderate CDOM levels. Note that radiation at lower wavelengths plays a greater role in the primary production process [30]. Values of the attenuation lengths used in the model for both Lake Erie and Lake Onego are listed in Table 2.1.

In addition to the modified absorption spectrum of CDOM dominated water, the distribution of the radiative flux throughout the water column can be further modified by the primary producers within [33]. The species of phytoplankton below the ice alongside their concentration will affect the optical properties of the water column (absorption spectrum of chlorophyll-a). We did not account for this added level of complexity and leave this as a suggestion for future work in the Conclusions section.

Simulations were performed with the (pseudo) spectral incompressible Navier-Stokes solver coined SPINS [53] in its DNS configuration. The equations of motion that are solved are the incompressible Navier–Stokes Equations under the Boussinesq approximation as outlined above (2.13-2.16). For temporal discretization, the code uses a third-order variable length time stepping method. Variable time steps are useful when dealing with flows that have a changing advective timescale over the course of the simulation (caused by

differences in velocity). A pseudo-spectral collocation method for spatial discretization is implemented, with the choice of spectral expansion depending on the desired boundary conditions. The 2-D simulations were configured with a domain that was rectangular in shape, with $(L_x, L_z) = (4.0, 8.0)$ m, and grid of $(N_x, N_z) = (2048, 4096)$ points, implying a resolution of 2 mm in both directions. The domain was periodic in the L_x direction and free slip (no flux) boundary conditions were applied at $z = 0, L_z$ to the velocity (temperature/dye) field. Note that SPINS uses a Fourier expansion for periodic boundary conditions, whereas a sine/cosine expansion is used in the case of free-slip boundaries [53]. Grid halving studies suggested that all results as reported in the following chapter are insensitive to grid refinement.

Spectral Band	**Lake Erie**	**Lake Onego**
Blue (400-500 nm)	$\xi_1 = 0.897\text{m}$ $(k_1 = 1.1145\text{m}^{-1})$	$\xi_1 = 0.200\text{m}$ $(k_1 = 5.0\text{m}^{-1})$
Green (500-600 nm)	$\xi_2 = 1.453\text{m}$ $(k_2 = 0.688\text{m}^{-1})$	$\xi_2 = 0.435\text{m}$ $(k_2 = 2.3\text{m}^{-1})$
Red (600-700 nm)	$\xi_3 = 0.943\text{m}$ $(k_3 = 1.060\text{m}^{-1})$	$\xi_1 = 0.714\text{m}$ $(k_3 = 1.4\text{m}^{-1})$

Table 2.1: Division of wavelengths into three bands across the PAR spectrum with corresponding attenuation lengths (coefficients) for both Lake Erie and Lake Onego. Attenuation constants were extrapolated from Twiss et al. [54] (see their Table 2) for Lake Erie, and from Bouffard et al. [9] (see their Figure 5a) for Lake Onego. The fraction of incoming radiation is split equally between the three bands, or equivalently, each irradiance constant has the same weight. When expressed as an attenuation length (units: m), the smaller the value, the faster that light attenuates within the water column.

We refrain from presenting the governing equations (2.13-2.16) in their dimensionless form as this thesis is focused on the presentation of physical results. Nevertheless, a brief discussion of the Reynolds number and Grashof number will be included in the following chapter to quantify the bulk properties of the flow. The Reynolds number is defined as

$$Re = \frac{UL}{\nu} \tag{2.18}$$

where Re gives the ratio of inertia to viscous terms. Here U and L represent problem specific velocity and length scales, respectively. The Grashof number, Gr, gives the ratio between buoyancy and viscous terms and is estimated as

$$Gr = \frac{\Delta\rho g L^2}{\nu U} \tag{2.19}$$

where $\Delta\rho$ is a typical, dimensionless density difference. We use the results of this non-dimensional analysis to comment on whether or not the turbulent scalings frequently applied in the RDC literature are valid (see, for example, [43], [32]).

2.3.1 Initialization and Experimental Design

All simulations are initialized from a linear temperature field

$$T(z) = \frac{(T_{top} - T_{bottom})}{L_z} z + T_{bottom} \tag{2.20}$$

starting with zero initial velocity ($\vec{u} = 0$). The parameter T_{top} sets the temperature of the upper water column at L_z, whereas T_{bottom} corresponds to the temperature at $z = 0$, that is, the bottom of the domain. The range of temperatures chosen are typical of late winter/early spring time conditions ([54], [9]) and are listed in Table 2.2 which outlines the cases considered in this thesis and their corresponding parameters. We consider these cases to identify how changes to under-ice irradiance (I_0) and the initial stratification affect the physical processes occurring within the water column over different time scales (day versus day/night, or diel cycles). Note that parameters that do not change across cases are commented on in the relevant sections of the text.

The concentration of phytoplankton, assumed nearly directly beneath the ice surface at the beginning of the simulation, is modelled by the dye field,

$$P(z) = \frac{1}{2}\left[1 + \tanh\left(\frac{z - 0.95L_z}{H}\right)\right] \tag{2.21}$$

where the width of the dye, H, was chosen arbitrarily as 0.01m.

The initial set up is schematized in Figure 2.2. As compared to the earlier Figure 1.2, we consider the point at which Winter I has just transitioned towards the second phase, namely, Winter II. Hence, we neglect heat transfer from the sediments meaning there are two avenues for energy exchange with the exterior environment. The first is an energy flux into the water by daily solar heating, the second is an energy loss to the ice due to heat fluxes through the diffusive boundary layer [56]. Recall that the convective mixed layer (grey region in Figure 2.2) is separated from the ice by this thin and stable layer. In its DNS configuration, SPINS is able to resolve all of the dynamics of interest, however, it cannot handle outward heat fluxes. Hence, we only consider incoming radiative fluxes in this thesis. It is important to note that what we call the convective mixed layer is not actually mixed at this point. Rather, we mean that the grey region of Figure 2.2 (which

encloses the domain extent) will experience mixing as the radiative forcing overcomes the density gradients and induces circulation within the water mass. In the absence of mixing, a quiescent under-ice water column is the common assumption in the literature ([33], [57], [34]). We represent this with a linear temperature profile beginning close to, but not exactly beneath the ice (SPINS has not been thoroughly tested to model $T = 0°\text{C}$).

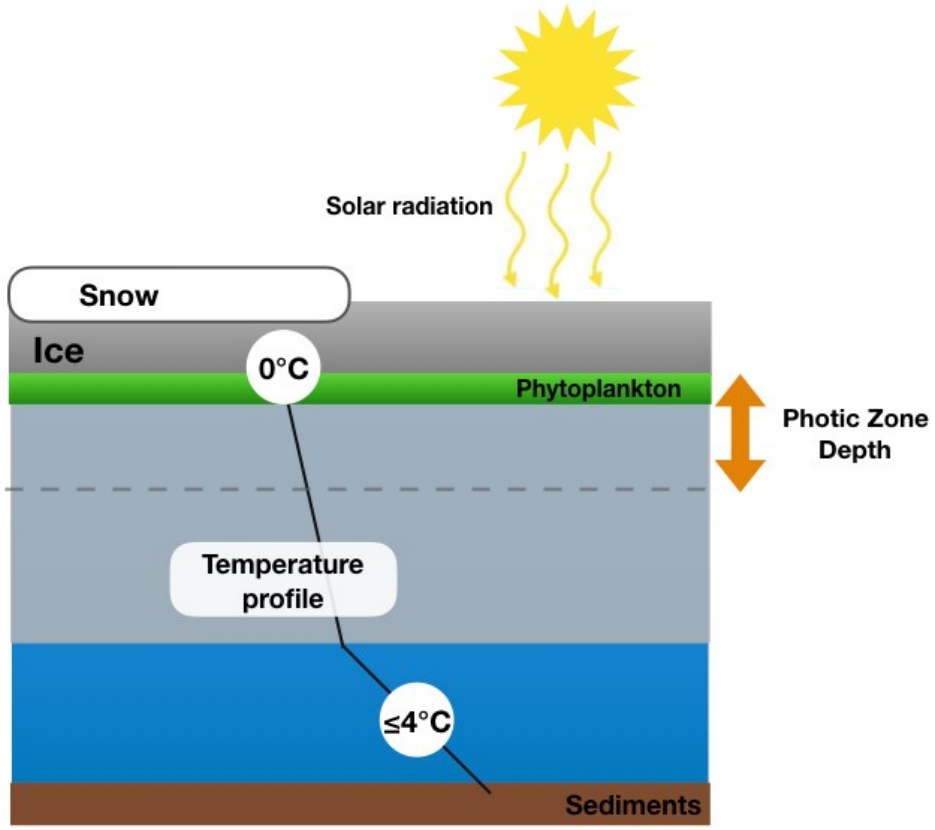

Figure 2.2: Schematic of the initial experimental set up. The grey region indicates the physical domain considered with assumed linear stratification. Phytoplankton are concentrated just beneath the ice surface where the depth of the photic zone is always less than the vertical extent of the domain. Heat flux from the sediments and through the ice layer are ignored. Increased solar radiation, due to reduced snow cover in late winter/early spring, is the driving force for under-ice convective motions.

Reduced snow cover in the early spring allows for increased primary productivity. In our model, we account for this as a thin layer of phytoplankton (more specifically, diatoms) just beneath the ice surface, near the top of the domain (see Figure 2.2). This assumption is valid as many field studies have found phytoplankton communities concentrated at the ice-water interface ([54], [45], [52]). The time scale all of simulations was short enough that we did not consider the growth and population dynamics of the winter diatoms which may be influenced by zooplankton grazing. Further to this, we refrained from modelling the sinking behaviour of diatoms given that the vertical (convective) velocities were found to be a few orders of magnitude larger than the associated sinking speeds of *Aulacoseira islandica* ($\approx 10^{-6}$ ms^{-1} [52]). Some exceptional phytoplankton species can regulate their buoyancy [47], allowing them a small level of control over their position in the water column. In line with the previous assumption of passivity, we ignore this level of detail and model the diatom species in question as neutrally buoyant, or completely non-motile. These points are reflected in Equation 2.16, which excludes a term to account for either population dynamics of plankton-induced motions.

Description	**Site Considered**	I_0 (Wm^{-2})	T_{top} ($^\circ C$)	T_{bottom}($^\circ C$)
No Stratification	Lake Erie	10	0.1	0.1
Linear Stratification	Lake Erie, Lake Onego	10	0.1	0.2
Increased Radiation	Lake Erie, Lake Onego	20	0.1	0.2
Diel Cycles	Lake Erie, Lake Onego	10	0.1	0.2

Table 2.2: Cases examined throughout this thesis, including a case description, the sites at which they are considered and their corresponding dimensional parameters. Note that the case with 'No Stratification' considers only the single lake. All parameters excluded from this table retain the same value throughout all simulations and are listed in the appropriate sections of the text.

2.3.2 Derived Diagnostic Quantities

Given that the initial state assumes a quiescent fluid, perturbations to the velocity field are governed by external forcing in the form of incoming solar radiation (see Equation 2.17). These convective motions drive changes in both the temperature and dye fields, as will be discussed in the subsequent Results section. Note that changes in temperature are directly influenced by the incoming solar radiation as well. In this thesis, particular focus is given to the distribution of phytoplankton throughout the water column, or alternatively, how

the dye is entrained by radiative forcing. The intensity of mixing in the water column is often less important to phytoplankton than the vertical depth through which they are mixed [47]. The primary requirement for a viable phytoplankton population to persist is prolonged residence in the lake's photic zone.

The depth of the photic zone for both Lake Erie and Lake Onego are shown in Figure 2.3. These depths were calculated from Equation 2.17 by setting the fraction of incoming under-ice radiation to 1% of its surface value and subsequently solving for the corresponding value of z. It is important to note that the photic zone may overlap with the convective mixed layer in the water column. Hence, the depth of entrainment by mixing is the major factor controlling the elimination of non-motile phytoplankton, such as diatoms. That is, if convective motions extend past the photic zone, phytoplankton may be pushed to depths greater than that at which they are able to photosynthesize and hence survive.

To quantify the concentration of phytoplankton (dye) within the photic zone at any given time, we let

$$P_{photic} = \int_0^{L_z} \int_0^{L_x} H(z - z_{critical}) P(x, z, t) dx dz \tag{2.22}$$

where $H(.)$ represents the indicator, or Heaviside step function. Here $z_{critical}$ corresponds to the depth of the photic zone for Lake Erie (5.39 m) or Lake Onego (2.57 m), depending on the lake in question, as these will be discussed separately in the Results section below.

Further relevant quantities are defined as follows:

$$ke(x, z, t) = \frac{1}{2}\left(u^2 + w^2\right), \tag{2.23}$$

$$T_{flux} = Tw \tag{2.24}$$

$$M_{flux} = uw. \tag{2.25}$$

Following standard practice, the kinetic energy (KE) is defined without the factor of ρ_0 in Equation 2.23. The temperature flux (2.24) describes how efficient the system is at moving heat downwards, whereas the momentum flux (2.25) gives the vertical flux of the horizontal momentum. In order to discuss the evolution of the system as a function of time and height, we let

$$\overline{KE}(z, t) = \frac{1}{L_x} \int_0^{L_x} ke dx \tag{2.26}$$

$$\overline{T_{flux}}(z, t) = \frac{1}{L_x} \int_0^{L_x} T_{flux} dx \tag{2.27}$$

$$\overline{M_{flux}}(z, t) = \frac{1}{L_x} \int_0^{L_x} M_{flux} dx. \tag{2.28}$$

Mean quantities, or rather, horizontal averages for the temperature and dye fields are defined analogously to the above. The averaged kinetic energy will be most important when considering the case of day/night (diel) cycles, where radiative forcing is effectively switched off after sunset. The remaining mean quantities are considered for the case of linear stratification only.

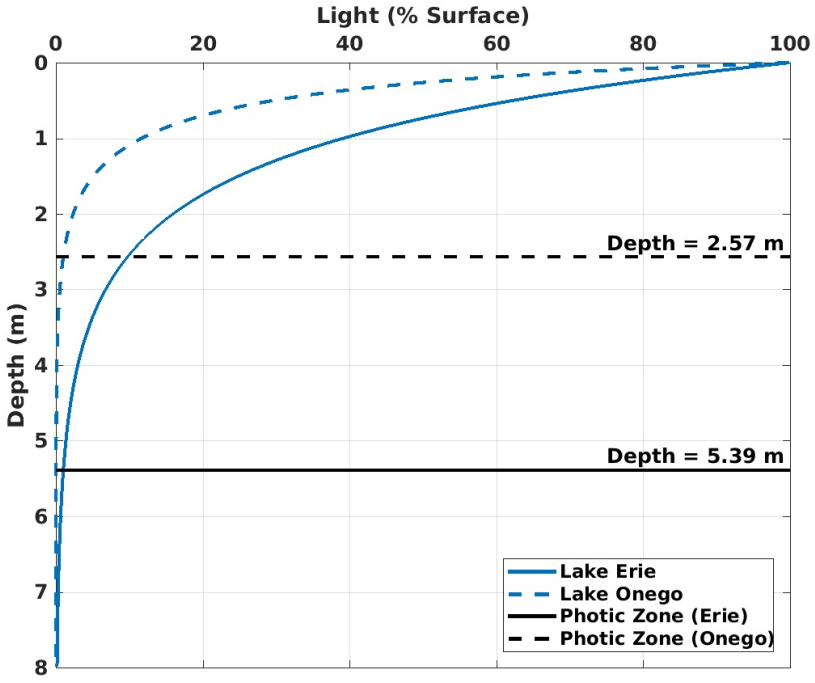

Figure 2.3: Light versus depth profiles for Lake Erie (moderate CDOM) and Lake Onego (high CDOM). The depth of the photic zone is delineated by the depth at which the amount of light available is reduced to 1% of the surface level. Note that the depth of the photic zone for Lake Erie is nearly twice that of Lake Onego, which strongly attenuates short wavelength (PAR) radiation in the first few metres of the water column under ice cover.

Chapter 3

Results and Discussion

In what follows, we analyze and discuss the results obtained for the cases as outlined in Table 2.2. We consider these cases to identify how changes to the initial stratification and the under-ice irradiance, I_0, affect the physical processes occurring within the water column over different time scales (day versus day/night, or diel cycles). All cases consider the dynamics associated with Lake Erie, followed by Lake Onego, save for the case of no stratification which focuses on Lake Erie only. Comparisons to Lake Onego serve to highlight the effects of increased CDOM levels on light attenuation and subsequently under-ice radiatively driven convection (recall that CDOM levels are on the rise in Lake Erie). The order of presentation begins with the case of no stratification, followed by that which considers a linear stratification. Next, we analyze the effects of increased solar radiation, or more specifically, increasing the under-ice irradiance, I_0, to double its previous value. Finally, we consider diel cycles, where radiative forcing is effectively switched off after sunset. The discussion focuses on coupled bio-physical lake processes whenever possible.

3.1 No Stratification

We begin with the somewhat unrealistic case of no stratification, considering only the under-ice optical environment of Lake Erie. Water quality profiles of the three basins in Lake Erie, as presented by Twiss et al. [54], show that it is not impossible for $T_{top} = T_{bottom}$, especially in mid-winter (see their Figure 4, panels (a) and (h)). Thus, using these profiles as a guide and again employing Ockham's razor, we begin our analysis with this simplified case. However, we quickly found that the front associated with the developing mixed

layer moved down quite fast over short time scales as compared to simulations with a pre-existing under-ice stratification; this is what motivated our initial use of word unrealistic. We discuss these dynamics briefly in what follows, quickly moving onto the case with more interesting results, namely, linear stratification.

Figure 3.1 depicts the evolution of the dye field in 45 minute intervals, starting from the initial quiescent state. Recall that the dye represents the concentration of non-motile diatoms in the water column. The dashed line indicates the extent of the photic zone, where the upper part of the domain corresponds to the region just beneath the ice-surface. Drawing our attention to panel (d), we see that shortly after $t = 180$ min (3 hours), diatoms are already being pushed past the photic zone to depths greater than that at which they are able to survive. Only 90 minutes later, the dye is smeared out over the entire domain, as outlined in panel (f). Essentially, this means that starting after sunrise, only four and half hours need to pass before radiative forcing drives motions to depths which encompass our entire domain extent. This is particularly troubling for phytoplankton as it implies that large portions of the population will be eliminated over the course of a single, sunny day. We refrained from running the simulations past the five hour mark ($t = 300$ min) for this reason.

If we consider the temperature field, we again note that the onset and development of the descending front driven by radiative convection moves quickly to the bottom of the domain. This is shown in Figure 3.2. Here the initial state at $t = 0$ has been subtracted off to best display the heating effects of radiatively driven convection in time. In panel (b), we observe convective plumes descending as mushroom-like fluid structures. This descent progresses feverishly, with temperature differences up to 0.02°C observed as early as panel (c) (this difference is contained in the vortex structure located mid-way through the domain). Similarly to the dye field, we see that the effects of radiative convection initiate heating down towards the bottom of the domain after only a short time ($t = 270$ min). The temperature field is not completely mixed out in panel (f), however, a significant portion of the 'lake' has experienced change.

The vertical velocity, w, indicates whether or not diatoms will be entrained by convective motions in the water column. As discussed in the Methods section, the sinking speeds of *Aulacoseira islandica* ($\approx 10^{-6}$ ms^{-1} [52]) found in Lake Erie are a few orders of magnitude smaller than the representative vertical velocities. These are on the order of 10^{-3} ms^{-1} as can be seen by the vertical scale of the colorbar in Figure 3.3. In the absence of a well-defined, under-ice stratification, we see that vertical motions become significant as soon as panel (c), or at $t = 135$ min. For the duration of the simulation, upward and downward motions are approximately equivalent over the domain extent. Significant convective regions appear in panel (e), and divide into smaller structures as time progresses

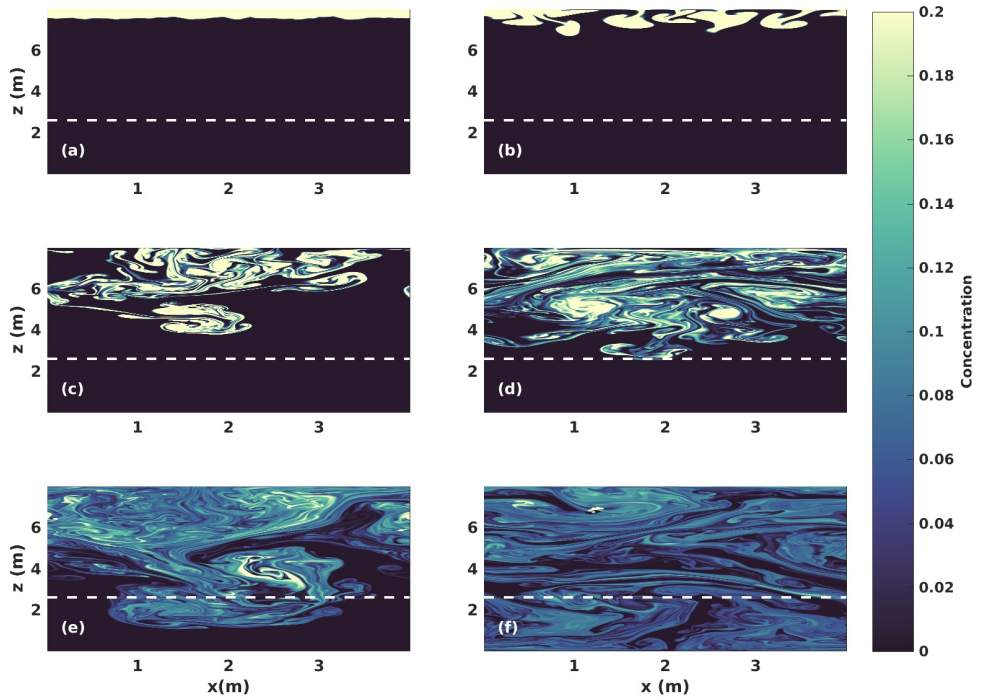

Figure 3.1: Evolution of the dye field in Lake Erie for the case of no stratification. The dye represents the concentration of non-motile diatoms in the water column. Dashed line indicates the extent of the photic zone, noting that the vertical axis is positive upwards (i.e. $z = 8$ m represents the near under-ice surface layer). Panels (a)-(f) correspond to the dynamics at 45 minute intervals, starting at (a) $t = 45$ min and ending at (f) $t = 270$ min.

(see panel (f)). Because motions appear to extend past the lower boundary of the domain in panel (f), we again stopped the simulation at the $t = 300$ min mark.

To quantify the concentration of phytoplankton within the photic zone at any given time, we consider the time series of the fraction of dye remaining in the photic zone of Lake Erie as shown in Figure 3.4. Consistent with Figure 3.1, we see that diatoms exit the photic zone starting around $t = 200$ min. Following this, there is a near exponential decrease until around $t = 275$ min, after which point the concentration of phytoplankton saturates near 0.65 at the time the simulation is terminated. Essentially, this implies that after only half a late winter/early spring day, close to one-third of the total diatom population will be

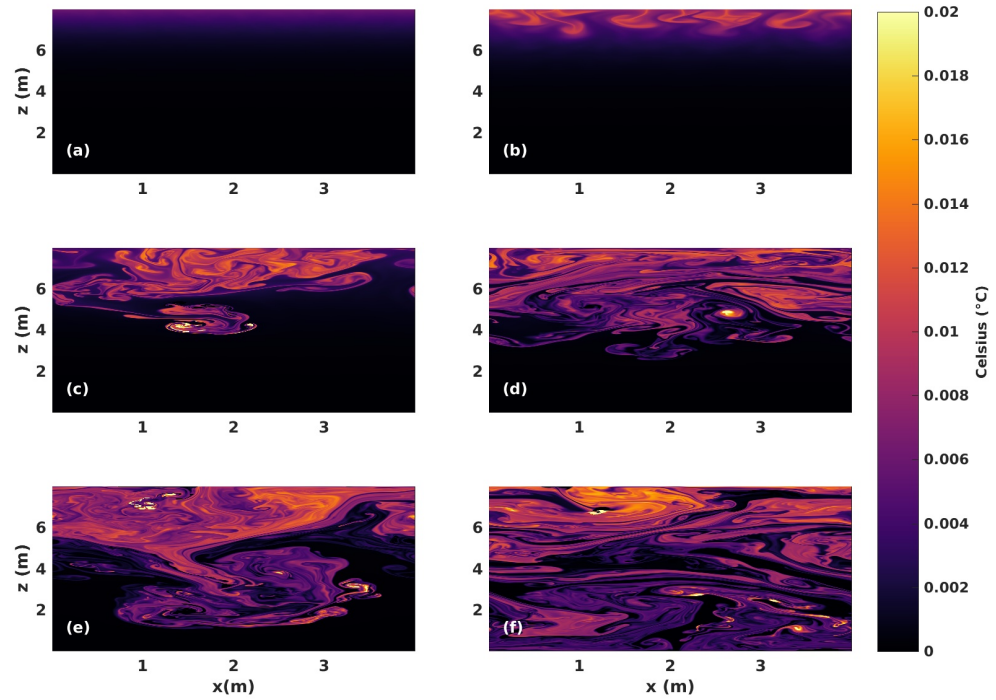

Figure 3.2: Evolution of the temperature field in Lake Erie for the case of no stratification. The initial state at $t = 0$ has been subtracted off in order to best show the onset and development of radiatively driven convection. Panels (a)-(f) correspond to the dynamics at 45 minute intervals, starting at (a) $t = 45$ min and ending at (f) $t = 270$ min.

eliminated from the water column. Note that we define the length of a single day in this thesis as the time for which forcing is active; this length is 10 hours for the remainder of all simulations, keeping in mind that we only ran the no stratification case for half of this time given the consistent overlap of the dynamics with the lower domain boundary. As we consider the case of a linear background stratification, we will more clearly understand the dire consequences for modelled phytoplankton when the temperature at the top and bottom of the domain (or lake, considering the physical problem) are set equal to one another. We consider this dynamically relevant case next, focusing on Lake Erie and Lake Onego in turn.

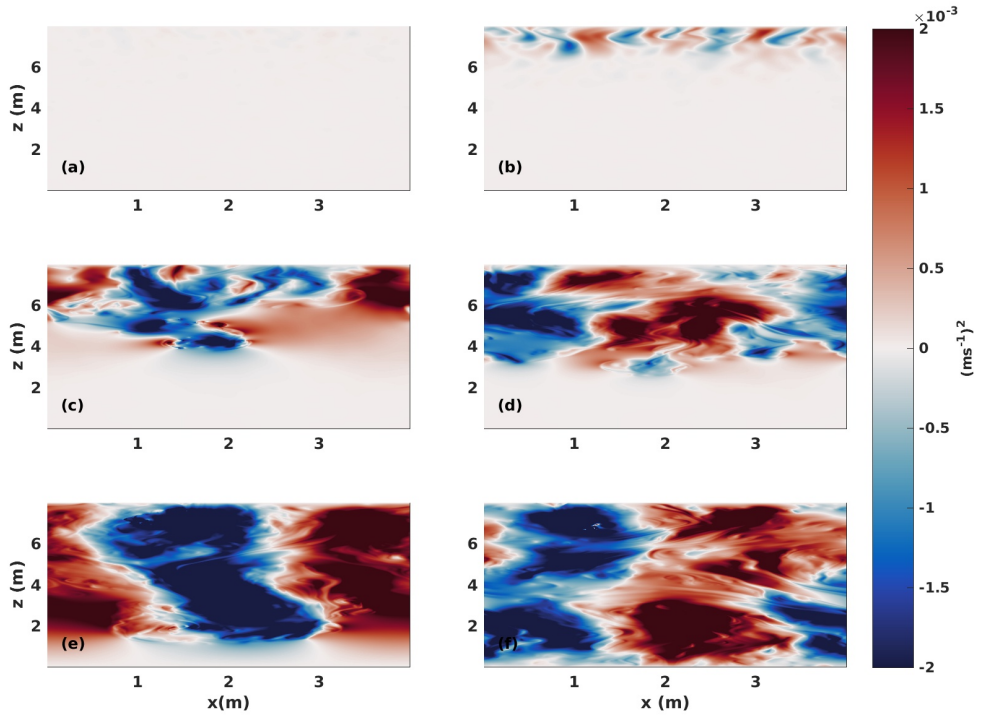

Figure 3.3: Evolution of the vertical (convective) velocity, w, in Lake Erie for the case of no stratification. Panels (a)-(f) correspond to the dynamics at 45 minute intervals, starting at (a) $t = 45$ min and ending at (f) $t = 270$ min. Note the small scale of the velocities.

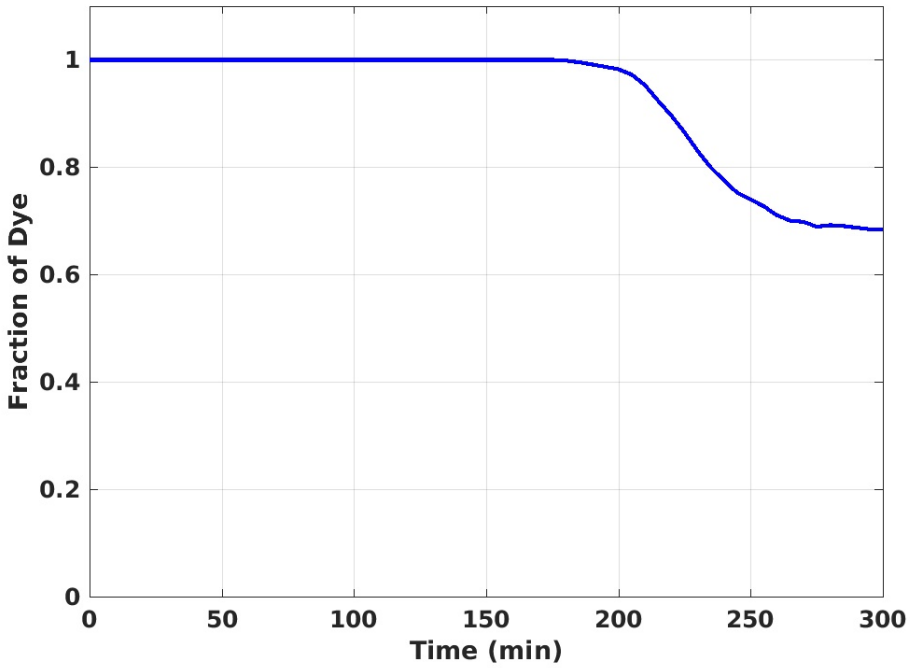

Figure 3.4: Time series of the fraction of dye remaining in the photic zone of Lake Erie for the case of no stratification. The total concentration of dye has been divided by its initial value to display the fractional change in time. Without stratification, close to one-third of all diatoms are removed from the photic zone by $t = 250$ min (just over 4 hours).

3.2 Linear Stratification

3.2.1 Lake Erie

Similar in presentation to the unstratified case above, we first consider the evolution of the dye field in Lake Erie as expressed in Figure 3.5. Keep in mind that the dye serves to model the concentration of non-motile diatoms in the water column. For the case of linear stratification, the simulation was run twice as long as compared to the case of no stratification. Thus, panels represent the dynamics at 90 minute intervals instead of the previous 45 minute increment. As before, the dashed line indicates the extent of the photic zone noting a key difference, namely, that the dye does not extend past this boundary for the duration of the simulation. In panel (c), the downward progression of diatoms in the water column is first prominent. The concentration of dye spreads gradually throughout the upper half of the domain and is neatly dispersed above the 4 m mark at $t = 540$ min (see panel (f)). The 2D plots shown here provide a qualitative view of the dynamics associated with the dye field. Below we will reconsider the distribution of phytoplankton in the water column more quantitatively, considering the horizontally averaged concentration of dye in space and time (see Figure 3.8).

Figure 3.6 depicts the evolution of the temperature field again in 90 minute intervals. The stable background stratification (representative of the initial state) has been subtracted off to show more clearly the onset and development of radiatively driven convection in waters with moderate CDOM concentrations. A significant build up of heat is evident in the upper layer starting in panel (d), or at $t = 360$ min. In time, the region beneath the ice-layer continues to warm up with temperature differences approaching 0.045°C by $t = 540$ min. The region of dominant heating is restricted to the upper few metres, yet non-negligible heating effects can be seen in the lower regions of the domain, most notably in the bottom right hand corner of panel (f). As with the dye field, we will consider the horizontally averaged temperature as a function of z and t further below (see Figure 3.9).

Vertical motions in the water column for the case of a linear background stratification are most pronounced in the surface layer. In Figure 3.7, we see alternating cells of upward and downward convective velocities as early as panel (c), with a similar behaviour extending until $t = 360$ min. Note that vertical velocities are again on the order of 10^{-3} ms^{-1} and thus, phytoplankton will be at the mercy of movements in the water column (fully entrained). Our simulations agree well with estimates of velocities in the convective mixed layer, which are assumed to be approximately 10^{-3} ms^{-1} as determined by different studies ([18], [33], [42]). As the simulation progresses, the dominant convective motions remain in the upper half of the domain with a change from small scale structures (panels (c) and (d)),

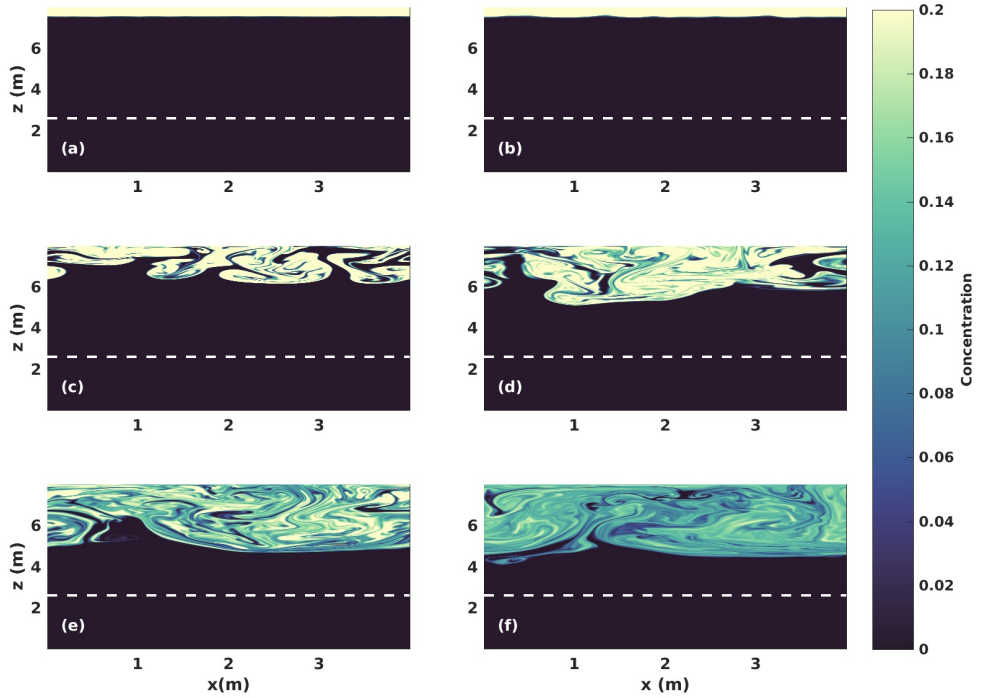

Figure 3.5: Evolution of the dye field in Lake Erie for the case of linear stratification. The dye represents the concentration of non-motile diatoms in the water column. Dashed line indicates the extent of the photic zone, which the dye does not leave throughout the length of the simulation. Panels (a)-(f) correspond to the dynamics at 90 minute intervals, starting at (a) $t = 90$ min and ending at (f) $t = 540$ min (9 hours).

to larger scale structures in panel (f). Most remarkable are the motions occurring in the stratified layer underneath the mid-point of the vertical axis. These undulating structures are visible in panels (e) and (f), and are unique to the case with linear stratification. In other words, such structures were not discernible in Figure 3.3. Descriptions of radiatively driven convection in the literature imply a well-mixed surface layer beneath the ice that increases in depth and penetrates into a stably stratified layer below. The motions associated with this penetration have, until now, been left to the imagination but here we are able to visualize their effects.

As alluded to above, we consider next the horizontal average of the dye field as a function

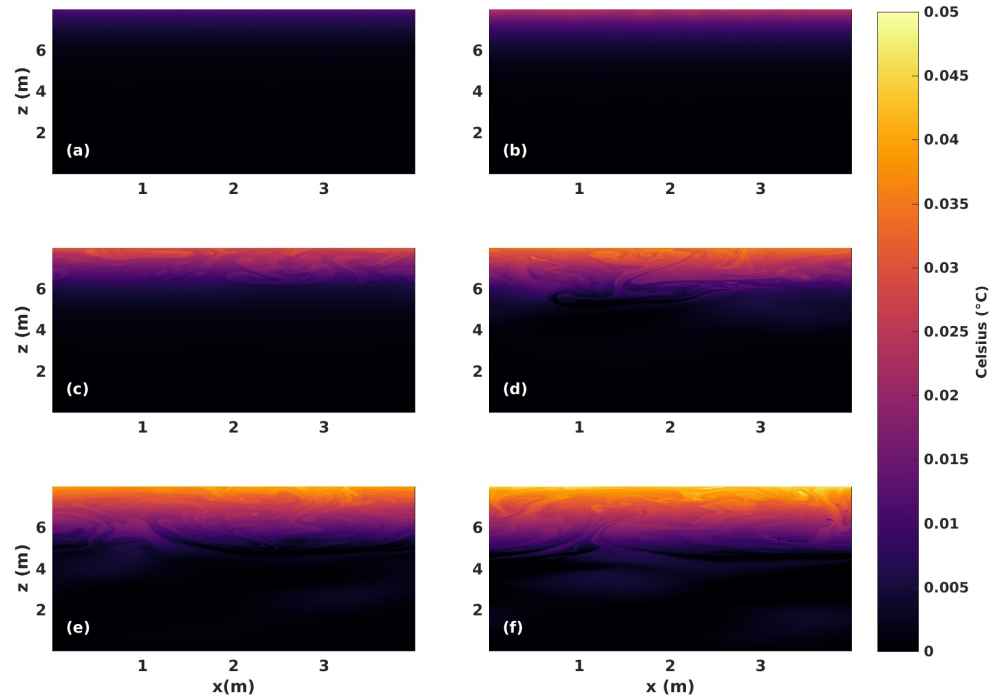

Figure 3.6: Evolution of the temperature field in Lake Erie for the case of linear stratification. The stable background stratification has been subtracted off in order to best show the onset and development of radiatively driven convection. Panels (a)-(f) correspond to the dynamics at 90 minute intervals, starting at (a) $t = 90$ min and ending at (f) $t = 540$ min (9 hours).

of space and time. In Figure 3.8 (a), we see the dispersion of the initial concentration of dye subject to radiative forcing over the course of a day ($t = 600$ min for these simulations). Prior to $t = 200$ min, the dye remains concentrated in the uppermost metre of the domain. Following this time, a dye front evolves and moves rapidly downward for approximately 100 minutes, after which time the front becomes less sharp. We estimate the speed with which the front moves downward (starting at $t = 300$ min and ending at $t = 600$ min) as approximately 0.11 mms^{-1}, or 4.02 md^{-1}, with the assumption of a ten hour day (here d^{-1} denotes per day). This can be understood as the rate of mixed layer deepening. In situ observations typically report CML-deepening rates of ≈ 0.5 md^{-1}; in the case of strong incoming solar radiation and a weak background stratification, the mixed layer can

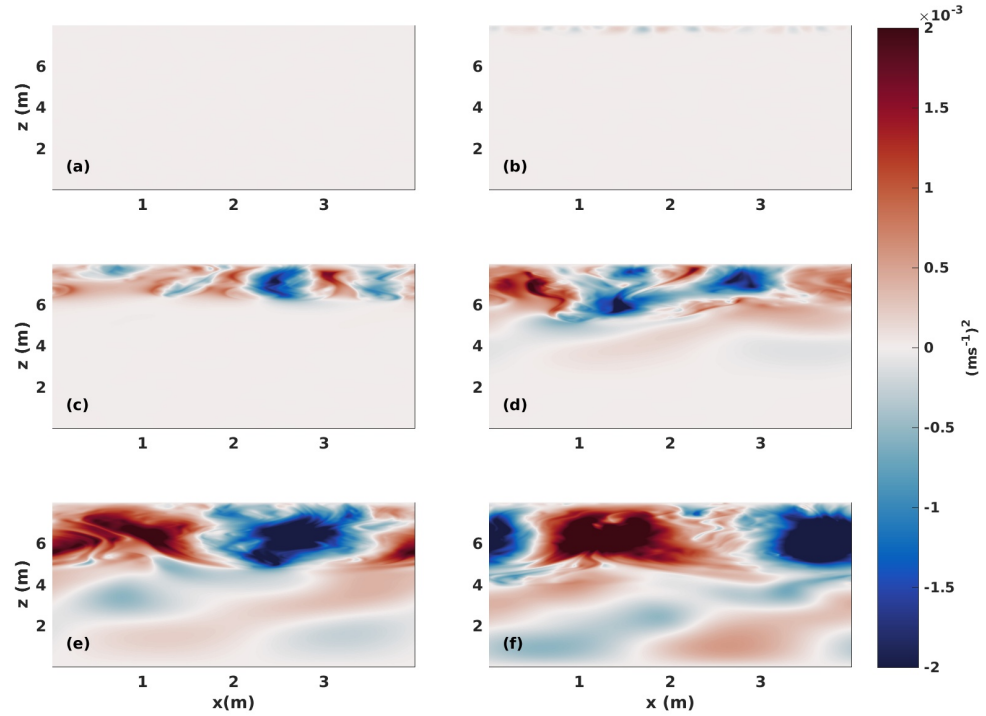

Figure 3.7: Evolution of the vertical (convective) velocity, w, in Lake Erie for the case of linear stratification. Panels (a)-(f) correspond to the dynamics at 90 minute intervals, starting at (a) $t = 90$ min and ending at (f) $t = 540$ min (9 hours). Note the change from small scale structures in panels (c) and (d) to large scale structures in panel (f).

advance at a rate of more than 3 md^{-1} [34]. It is important to note that most studies of radiatively driven convection in the literature assume that the CML already exists, whereas in this work, it is just developing. Nevertheless, our approximate estimate of 4.02 md^{-1} is consistent with the reported value of more than 3 md^{-1}. This makes sense given the weak background stratification, that is, the 0.1°C change over 8 m (or 0.125°Cm^{-1}). To observe the dynamics at individual times, panel (b) outlines the concentration of dye as a function of z for the six distinct times as highlighted by the coloured vertical lines in panel (a). The dashed line in the lower panel indicates the extent of the photic zone. Notably, the dye does not extend past this region for the length of the simulation, implying that phytoplankton are quite safe in Lake Erie for the case of an assumed linear stratification.

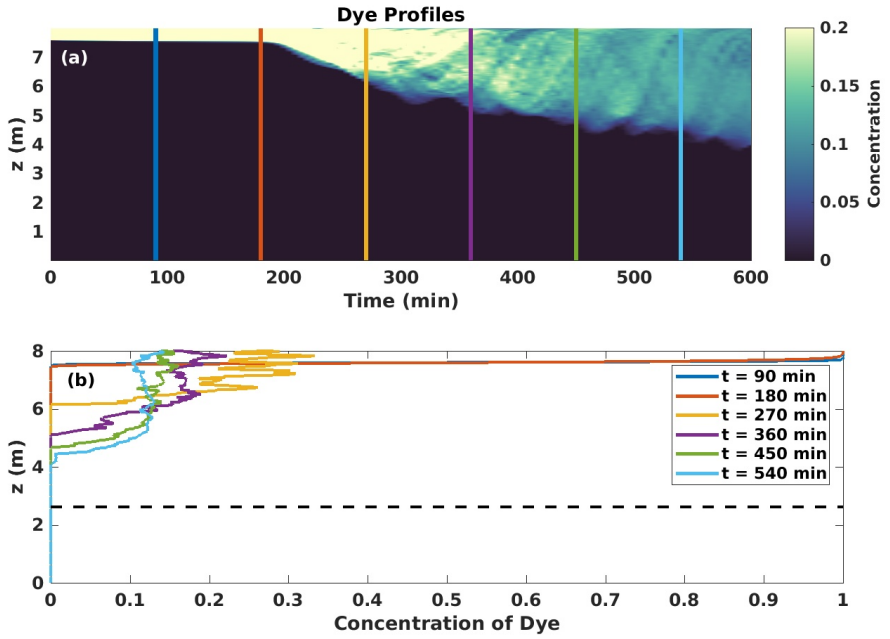

Figure 3.8: (a) Horizontal average of the dye field as a function of z and t in Lake Erie for the case of linear stratification. Note that the vertical axis is positive upwards. Coloured lines overlying the dye profiles correspond to the times displayed in the panels of the 2D evolution plots (i.e. vertical lines mark the passage of 90 minute intervals). (b) The concentration of dye as a function of z for the various times (indicated by colour) highlighted in panel (a). The dashed line outlines the extent of the photic zone for Lake Erie.

The upper panel of Figure 3.9 displays the horizontal average of the temperature field as a function of z and t. As before, the background stratification has been subtracted in order to show the effects associated with radiatively driven convection over the course of the simulation. Heating occurs almost exclusively in the upper 3.5 m of the domain, with temperature differences reaching as high as 0.04°C in the top, right hand corner at $t = 600$ min. Over most of the domain, however, temperature differences are on the order of 0.015°C (hazy purple regions) in the developing mixed layer. This average value agrees well with that reported by Forrest et al. [19], who found that the CML warmed at $0.015°\text{Cd}^{-1}$ during the observation period of their field study. Shifting our attention to panel (b), we see the stratification profiles corresponding to the various times (indicated by colour) in panel (a). Note that the lower panel for the temperature plots contrasts the pattern of the horizontally averaged figures. That is, rather than depict the exact dynamics as observed

in panel (a) at discrete times, panel (b) displays unique dynamics, namely, stratification profiles. This difference in presentation will be encountered again for Lake Onego when considering the one-dimensional temperature plots.

Depiction of the stratification profiles as in Figure 3.9 (b) is particularly interesting as it allows us to discern whether or not the convective mixed layer structures itself as expected in the literature. Recall from the Introduction that it is generally accepted that as warmed, heavier parcels of water sink, a convective mixed layer (CML) of approximately uniform temperature and density forms which deepens in time [34]. The CML is separated from the ice by a thin, stable diffusive layer and lies above a quiescent layer which increases in temperature downwards toward the sediment. Given the depth and time scale of our current simulations, we are unable to completely resolve either of these regions (see directly beneath the ice surface and the purple region of Figure 1.2 (b)). Nevertheless, we can comment on the development of the convective mixed layer and confirm whether or not the assumption of uniformity is accurate. At $t = 180$ min, only three hours after convective forcing begins, we see a clearly unstable region contained within a 1 m region below the surface. As time progresses, this somewhat erratic profile is replaced by nearly, but not completely well mixed stratification profiles (for example, see the curve associated with $t = 540$ min). To assume that the mixed layer deepens in time is completely correct, given the lengthening of the stratification profiles over time. However, the temperature fluctuations in each profile, though small, are not negligible. Thus, to say that the CML is uniform in both temperature and density is not consistent unless the word approximately is stressed. The trend in time does seem to move towards smoother, more uniform profiles, as can be seen by comparing curves at $t = 360$ min and $t = 450$ min. However, longer runs must be considered to verify this conjecture.

It was mentioned in the Methods section that profiles of the kinetic energy would be most important when considering the case of diel cycles, where radiative forcing is effectively switched off after sunset. While this statement remains true, we briefly look at the kinetic energy dynamics as occur under constant forcing. In Figure 3.10 (a), we see the horizontal average of the kinetic energy as a function of space and time. Up until $t = 360$ min, there is little motion and what does occur past this point is mainly restricted to the upper half of the domain. Starting just before $t = 450$ min, we see a noticeable increase in kinetic energy that moves downward in time, as highlighted by the bright yellow region snaking across the domain. More detailed dynamics are visible in panel (b), where again for late times ($t = 450$ min and $t = 540$ min), the kinetic energy has significantly increased. Associated with these strong convective motions are weaker but non-zero motions in the stratified layer, that is, below the 4 m mark. It is important to note the scale of the horizontal axis, namely, that all values are multiplied by a factor of 10^{-6}. Hence, the

observed values of kinetic energy are consistent with currents on the order of 1 mms^{-1}.

Values associated with the momentum flux are of the same order as the kinetic energy. Given this, it is worth drawing attention to the vertical scale of the colorbar in Figure 3.11, panel (a), which is presented as an order of magnitude smaller (10^{-7}) than that of Figure 3.10 (a). The choice of colorbar limits for the current axes were chosen by trial and error to enhance the presentation of the dynamics. Recall that the momentum flux gives the vertical flux of the horizontal momentum and is most useful to display different types of motion as they occur over the domain extent. In panel (a), we see that after approximately $t = 270$ min, there is a consistent transfer of momentum to lower layers. In the developing convective mixed layer, there is both upward and downward transport, but the stratified region beneath is mainly positive; this is most notable for times succeeding $t = 360$ min. These patterns are most clearly seen in panel (b). By considering the individual curves for $t = 360$ min through to $t = 540$ min, we see the fluctuation between positive and negative values in the upper half of the domain, followed by the adoption of strictly positive values below the 4 m mark.

For the purpose of this thesis, it is important to track how temperature distributes itself vertically throughout the water column; this has direct implications for primary producers. The non-linear term on the left-hand side of Equation 2.15 (considering vertical momentum only) describes how efficient the system is at moving heat downwards. This temperature flux is the last quantity we consider to describe the under-ice dynamics occurring in Lake Erie. In panel (a) of Figure 3.12, we see that downward motions begin around $t = 180$ min which increase in strength and depth as the simulation progresses. Specifically, at $t = 360$ min, and again at $t = 450$ min there are strong pulses of downward movement. The upper half of the domain displays this characteristic downward behaviour, but the dynamics at greater depths are particularly fascinating. Starting at approximately $t = 300$ min and continuing until the simulation is terminated at $t = 600$ min, there are consistent alternating upward and downward fluctuations experienced beneath the convective front. This striped pattern is indicative of wave motion (gravity waves) in the lower, stratified layer. In panel (b), this can be seen as modulations in the lower half of the domain for the green and blue curves, corresponding to $t = 450$ min and $t = 540$ min, respectively.

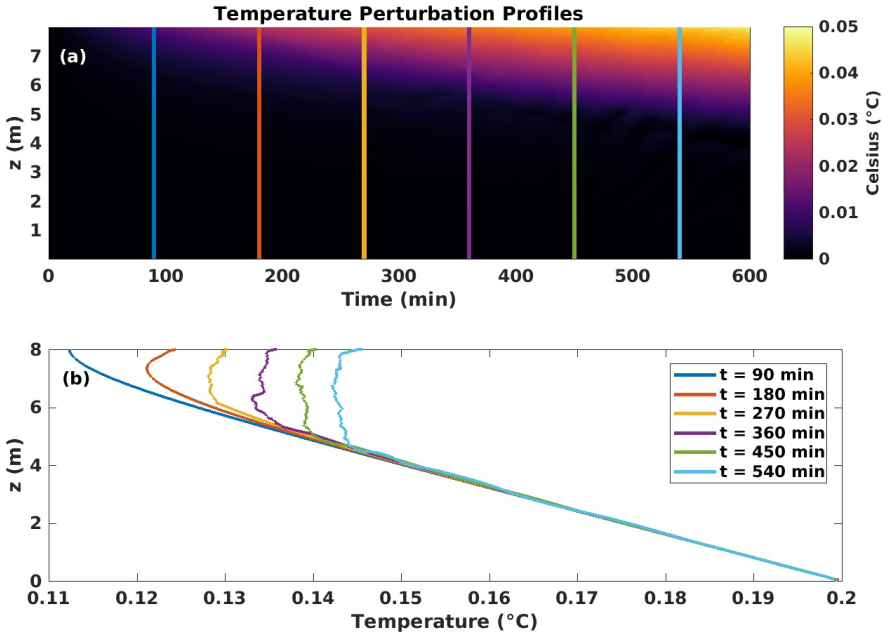

Figure 3.9: (a) Horizontal average of the temperature field as a function of z and t in Lake Erie for the case of linear stratification. The stable background stratification has been subtracted off to best display the heating effects of radiatively driven convection in time. Coloured lines overlying the temperature profiles correspond to the times displayed in the panels of the 2D evolution plots (i.e. vertical lines mark the passage of 90 minute intervals). (b) Stratification profiles corresponding to the various times (indicated by colour) shown in panel (a). At late times, we see the development of a nearly isothermal region in the upper 3 m of the water column.

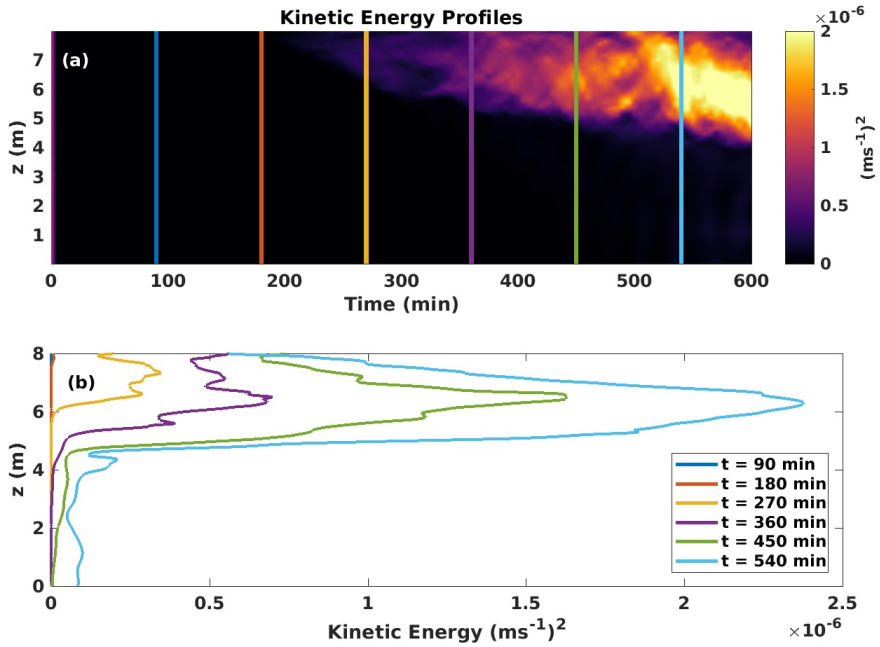

Figure 3.10: (a) Horizontal average of the kinetic energy as a function of z and t in Lake Erie for the case of linear stratification. Coloured vertical lines mark the passage of 90 minute intervals. Up until $t = 360$ min, there is little motion and what does occur past this point is mainly restricted to the upper half of the domain. (b) Kinetic energy profiles corresponding to the various times (indicated by colour) as shown in panel (a). Observed values of kinetic energy are consistent with currents on the order of 1 mms^{-1}.

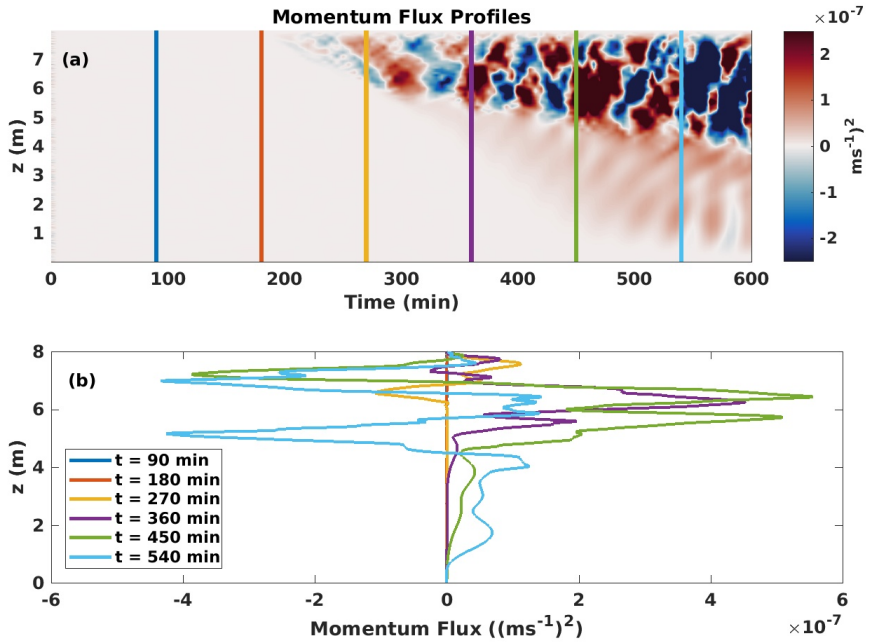

Figure 3.11: (a) Horizontal average of the momentum flux as a function of z and t in Lake Erie for the case of linear stratification. Coloured vertical lines mark the passage of 90 minute intervals. After $t = 270$ min, there is a consistent transfer of momentum to lower layers. (b) Momentum flux profiles corresponding to the various times (indicated by colour) as shown in panel (a). On average, the momentum flux is dominated by positive values, where a shift in this behaviour begins around $t = 540$min.

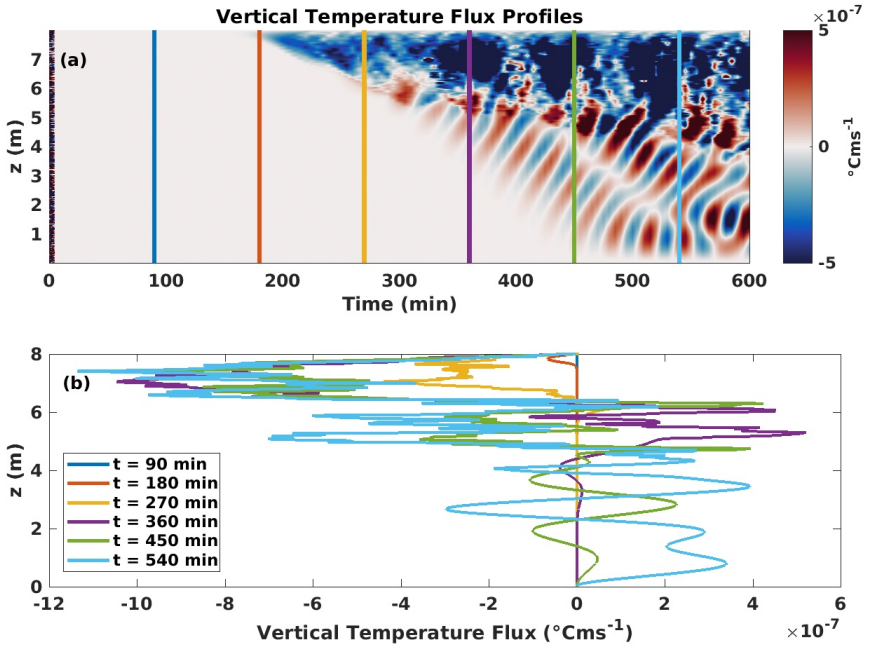

Figure 3.12: (a) Horizontal average of the vertical temperature flux as a function of z and t in Lake Erie for the case of linear stratification. Coloured vertical lines mark the passage of 90 minute intervals. Around $t = 360$ min and again at $t = 450$ min are strong pulses of downward movement. (b) Vertical temperature flux profiles corresponding to the various times (indicated by colour) as shown in panel (a). The temperature flux is solely negative in the upper few metres of the domain with small and consistent positive fluctuations experienced in the lower reaches.

3.2.2 Lake Onego

We examine next Lake Onego to compare and contrast the effects of increased CDOM levels on light attenuation and subsequently under-ice radiatively driven convection. Recall that the difference in CDOM concentration is reflected by differing attenuation lengths (coefficients) in our model (see Table 2.1). Overall, the attenuation lengths associated with Lake Onego are much smaller than Lake Erie; this implies that light will be absorbed much faster within the water column (meaning more heat in a smaller, near surface area), with the added implication of a shallower photic zone (refer to Figure 2.3). As we demonstrate below, the high levels of coloured dissolved organic matter in Lake Onego have dire consequences for phytoplankton development. Note that aside from the attenuation coefficients, all other parameters are considered equal to the case of Lake Erie as described above (i.e. linear stratification, $I_0 = 10$ Wm^{-2}).

The evolution of the dye field in Lake Onego is shown in Figure 3.13, where as before, the panels represent the dynamics at 90 minute intervals. The dashed line indicates the extent of the photic zone, which is much closer to the region below the ice surface than in the case of Lake Erie. The descent of diatoms in the water column is much faster as compared to Lake Erie, where plumes of downward motion are visible as early as 90 minutes into the simulation (see panel (a)). Recall that the downward progression of diatoms was first prominent at $t = 270$ min in Lake Erie. Another key difference to note is that the dye passes out of the photic zone in Lake Onego, with the first diatoms being eliminated shortly after $t = 180$ min. Following this point, the concentration of dye is smeared throughout the upper half of the domain, reaching depths just below 4 m in panel (f). Note that the concentration of phytoplankton in Lake Onego is more uniform, or well-mixed, throughout the upper confines of the domain than in Lake Erie (compare to Figure 3.5, specifically panels (e) and (f)). Similar to the presentation above, we reconsider the distribution of phytoplankton in the water column of Lake Onego more quantitatively (see Figure 3.16).

Figure 3.14 depicts the evolution of the temperature field again in 90 minute intervals. The stable background stratification (representative of the initial state) has been subtracted off to show more clearly the onset and development of radiatively driven convection in waters with high CDOM concentrations. Significant heating effects occur as soon as panel (c), or at $t = 270$ min, which is faster than occurs in Lake Erie (compare to Figure 3.6 (d)). Strong light attenuation in the upper layers of the water column cause drastic heating directly beneath the ice surface, as seen in panel (f), with temperature differences approaching 0.05°C. Dominant heating effects extend to a depth of 4 m over the course of the simulation. In panels (e) and (f), we note small contributions of the heat flux in the lower portion of the domain, restricted near the lateral boundaries. Such

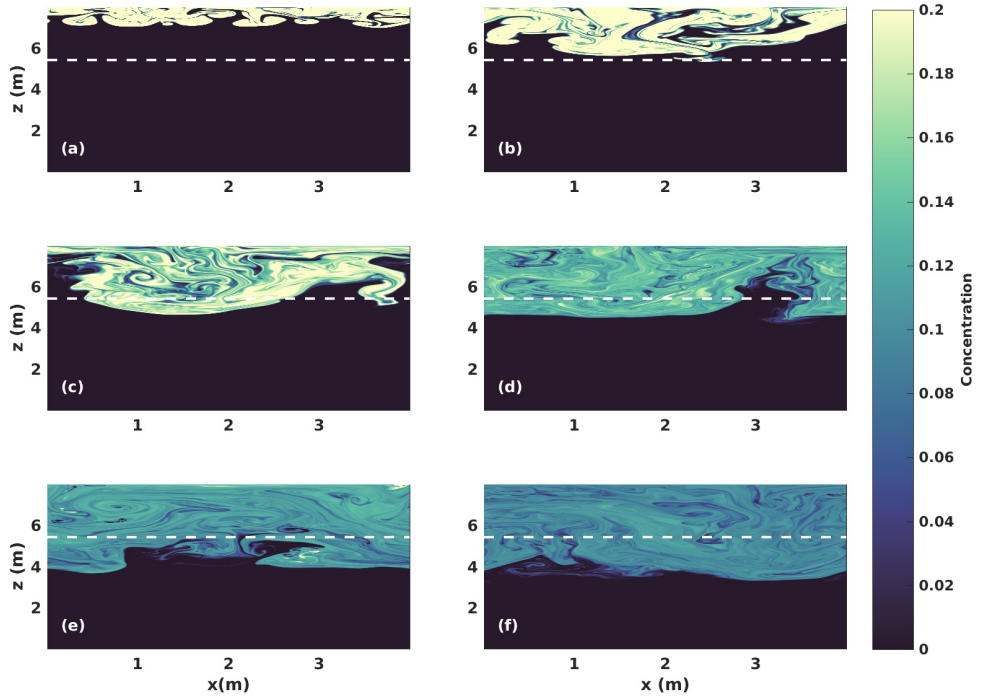

Figure 3.13: Evolution of the dye field in Lake Onego for the case of linear stratification. The dye represents the concentration of non-motile diatoms in the water column. Dashed line indicates the extent of the photic zone, through which the dye penetrates noticeably in panel (c). Panels (a)-(f) correspond to the dynamics at 90 minute intervals, starting at (a) $t = 90$ min and ending at (f) $t = 540$ min (9 hours).

behaviour was not noticeable in Lake Erie for panel (e) of Figure 3.14, and what small heating effects were visible in panel (f) were of considerably lesser magnitude (0.001°C versus 0.01°C as seen here). On par with the dye field, we will consider the horizontally averaged temperature as a function of z and t further below (see Figure 3.17).

Lake Onego boasts significant vertical motions in the water column, with convective cells first visible as soon as $t = 90$ min as seen in Figure 3.15, panel (a). Alternating cells of upward and downward convective velocities occur over the course of the simulation with a transition from small scale structures at earlier times, to large scale structures nearing the end of run time (compare panels (a) and (f)). As with Lake Erie, the vertical velocities

are on the order of 10^{-3} ms^{-1} and thus, phytoplankton will be fully entrained. However, the range of vertical motion through which the phytoplankton may be displaced is much larger than for Lake Erie, as evidenced by contrasting with Figure 3.7. Similar to Lake Erie, motions occur in the stratified layer, or the lower reaches of the domain. The motions as visible in the bottom 3 m of Figure 3.13, particularly panel (f), exhibit less rolling, or wave-like behaviour as those that were seen to occur in Lake Erie.

The horizontal average of the dye field as a function of space and time in Lake Onego is shown in panel (a) of Figure 3.16. The initial concentration of dye begins to spread downwards as early as $t = 75$ min, and exhibits rapid movement for approximately 50 minutes. Following this time, the front becomes less pronounced. As with Lake Erie, we can estimate the speed with which the front moves downward (starting at $t = 150$ min and ending at $t = 600$ min) as approximately 0.14 mms^{-1}, or 4.98 md^{-1}, with the now common assumption of a ten hour day. Note that the rate of mixed layer deepening is slightly faster (by roughly 30%) in Lake Onego, and that the dispersion of dye throughout the domain occurs 150 minutes sooner than was seen for Lake Erie in Figure 3.8. Bouffard et al. [9] estimated the deepening of the convective mixed layer in Lake Onego during the late winter period of 2017 as 1.0 ms^{-1}, three orders of magnitude larger than our approximate value. Some caution should be exercised in comparing this value to the one revealed by our simulations given the author's use of a relational equation that employs the buoyancy flux and background stratification of the water column. Note that the buoyancy flux depends on the absorption of incoming under-ice radiation in the mixed layer. For the 2017 campaign [9], the value for I_0 was quoted as approximately an order of magnitude greater than the value used in these simulations, which helps to explain the (large) discrepancies between measured values. Note that we based our estimate of $I_0 = 10$ Wm^2 on the 2016 field campaign of Bouffard et al. [9] for which a rate of mixed layer deepening was not quoted (see Table 1 in [9]). Nevertheless, it is clear that the rate of mixed layer deepening in lakes with high levels of CDOM are larger than those with only moderate concentrations (contrasting again with Lake Erie). Of course, this has direct implications for primary producers. Panel (b) of Figure 3.16 represents the depth of the photic zone with a dashed line and allows us to observe the effects of a deepening mixed layer on diatom development. For all times after $t = 180$ min, some concentration of dye dives below the photic zone meaning that diatoms are less likely to survive on longer time scales in lakes that experience high light attenuation, and hence, shallower photic zones.

The upper panel of Figure 3.17 displays the horizontal average of the temperature field as a function of z and t. Consistent with the presentation above, the background stratification has been removed in order to show the effects associated with radiatively driven convection over the course of the simulation. As with Lake Erie, heating is mainly

concentrated in the top portion of the domain. However, for the case of Lake Onego, heating effects are experienced sooner (starting at $t = 75$ min) and temperatures differences reach values as high as 0.05°C for late times (see the upper, right-hand corner of panel (a)). Overall, the heat contributions associated with radiatively driven convection are more pronounced in lakes with high CDOM concentrations, as compared to those with moderate levels (compare with Figure 3.9). Shifting our attention to panel (b), we see the stratification profiles for Lake Onego corresponding to the various times (indicated by colour) in panel (a). Recall that in the case of Lake Erie, a clearly unstable region contained within a 1 m region below the surface became visible at $t = 180$ min. A similar structure is observed in Lake Onego but at an earlier time, namely $t = 90$ min, as traced out by the dark blue, leftmost curve in the lower panel. In time, this unstable curve is replaced with nearly, but not completely well mixed stratification profiles (see for example $t = 450$ min). Most notable is the hook-like structure that appears in the underlying stratification at late times. That is, we see the development of a nearly isothermal region extend below a sharply decreasing surface layer of approximately unit height. Beneath this isothermal region, the stratification gets stretched downwards and to higher temperatures before resuming a linear increase. For the clearest visualization of this phenomenon, which is unique to the case of Lake Onego, see the curve associated with $t = 540$ min.

We briefly consider the kinetic energy as occurs under constant forcing in Lake Onego, noting that a comprehensive analysis of the kinetic energy dynamics will be addressed for the case of diel cycles further below. In Figure 3.18 (a), we see the horizontal average of the kinetic energy as a function of space and time. Motion persists in the upper half of the domain starting shortly after $t = 90$ min, and extends rapidly downwards, just shy of the 3 m mark at late times. Note that motions appear in the upper water column approximately 150 minutes sooner in Lake Onego than in Lake Erie (compare to Figure 3.10). Heightened values of kinetic energy appear as bursts in localized regions first at $t = 450$ min and again at $t = 540$ min. More detailed dynamics are visible in panel (b). We note the significant increase in kinetic energy at late times, particularly the scale of motion at $t = 450$ min and $t = 540$ min, consistent with our previous observation. Associated with these strong convective motions, are weaker, but non-zero motions in the underlying stratified layer. These small amplitude motions appear to occur for all times past $t = 360$ min. Similar to Lake Erie, the observed values of kinetic energy are consistent with currents on the order of 1 mms^{-1}.

As before, we present the momentum flux which gives the vertical flux of the horizontal momentum, only now with focus on Lake Onego. In Figure 3.19 (a), we see that after approximately $t = 100$ min, there is a consistent transfer of momentum to lower layers, exhibiting both upward and downward motions. Compared to Lake Erie (see Figure 3.11

(a)), this momentum transfer exists across longer time scales, or rather, motions are significant across a larger extent of the horizontal domain. Another notable difference is the shift of momentum away from the near ice-surface layer in Lake Onego. At late times (starting at approximately $t = 500$ min) there is very little motion in a thin region near the upper, right-hand corner of the domain. Such behaviour did not occur in Lake Erie, where convective cells extended to full height (see again Figure 3.11). Focusing our attention now to lower regions, we see that at late times, there are less coherent motions in the stratified layer of Lake Onego (lower 4 m of the domain) compared to those that were seen in Lake Erie. In further contrast, what little motions do extend to this depth can take on both positive and negative values (recall that in Lake Erie, such motions were strictly positive). This is most clearly seen in panel (b), where the curves associated with $t = 450$ min and $t = 540$ min fluctuate around zero below the 4 m mark.

Lastly, we consider the horizontal average of the vertical temperature flux as a function of z and t in Figure 3.20 (a). Similar to Lake Erie (compare to Figure 3.12), the upper half of the domain displays a characteristic downward trend, although the structures in this region differ slightly (less concentrated in Lake Onego). Furthermore, this downward flux begins sooner than observed in Lake Erie, with dark blue plumes visible by $t = 75$ min. It is important to note that when comparing to the case of Lake Erie, the vertical scale of the colorbar in Figure 3.20 panel (a), is an order of magnitude larger (10^{-6}) than that of Figure 3.12. Although perhaps not the best for direct comparison, this choice of scale most clearly reflected the vertical temperature flux profiles of Lake Onego. This difference in order of magnitude is also reflected in panel (b). Consistent alternating upward and downward fluctuations appear beneath the convective front, where as in Lake Erie, this striped pattern is indicative of wave motion in the lower, stratified layer. An important note is that these wave-like motions occur over longer timescales in lakes with high levels of CDOM as compared to those that host only moderate concentrations (their appearance is notable approximately 180 minutes, or 3 hours sooner). These modulations are clearly seen in the lower half of the domain in panel (b). Wave-like motions become first apparent at $t = 270$ min and continue for all curves representative of times thereafter.

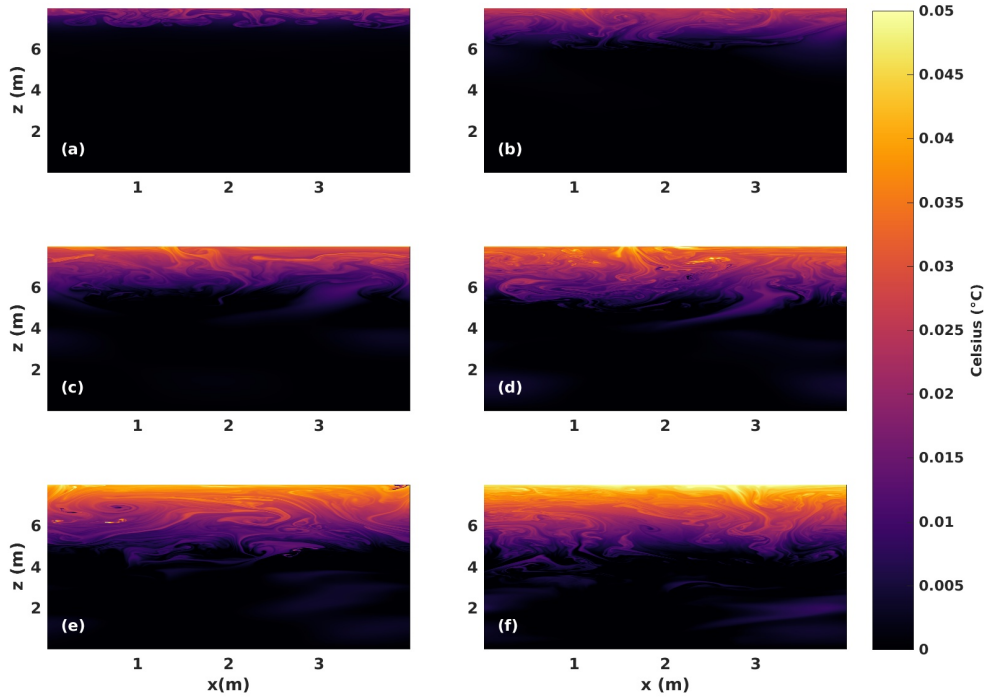

Figure 3.14: Evolution of the temperature field in Lake Onego for the case of linear stratification. The background stratification has been subtracted off to best display the heating effects of radiatively driven convection in time. Note the increased near-surface heating, consistent with high CDOM concentrations as observed in this lake. Panels (a)-(f) correspond to the dynamics at 90 minute intervals, starting at (a) $t = 90$ min and ending at (f) $t = 540$ min (9 hours).

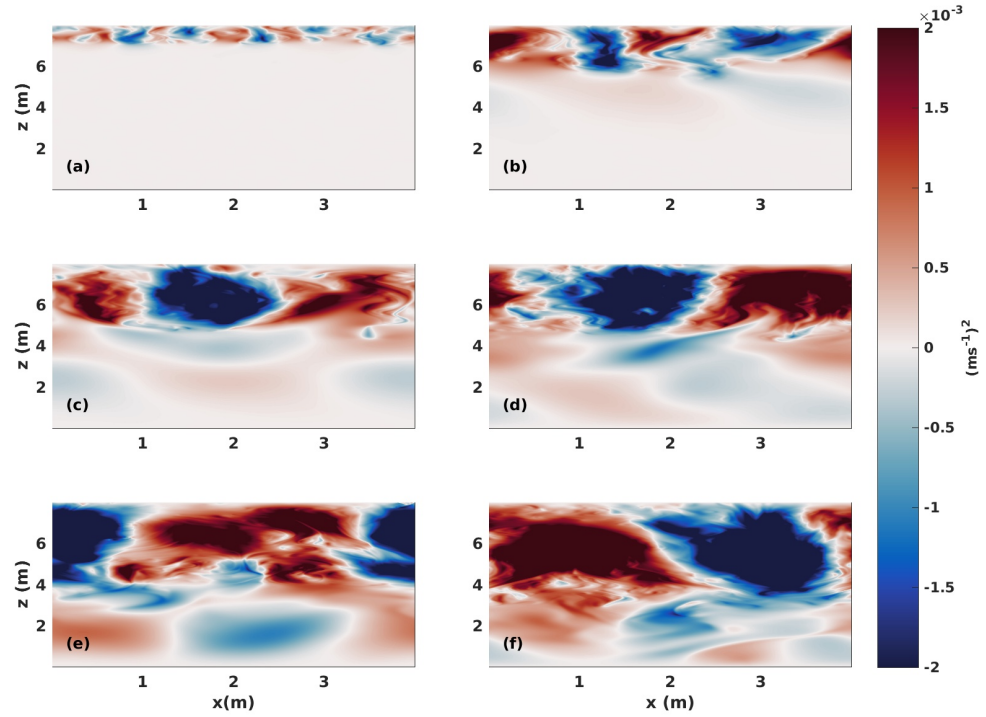

Figure 3.15: Evolution of the vertical (convective) velocity, w, in Lake Onego for the case of linear stratification. Panels (a)-(f) correspond to the dynamics at 90 minute intervals, starting at (a) $t = 90$ min and ending at (f) $t = 540$ min (9 hours). Large scale structures appear as early as panel (c) and increase significantly approaching the end of the simulation.

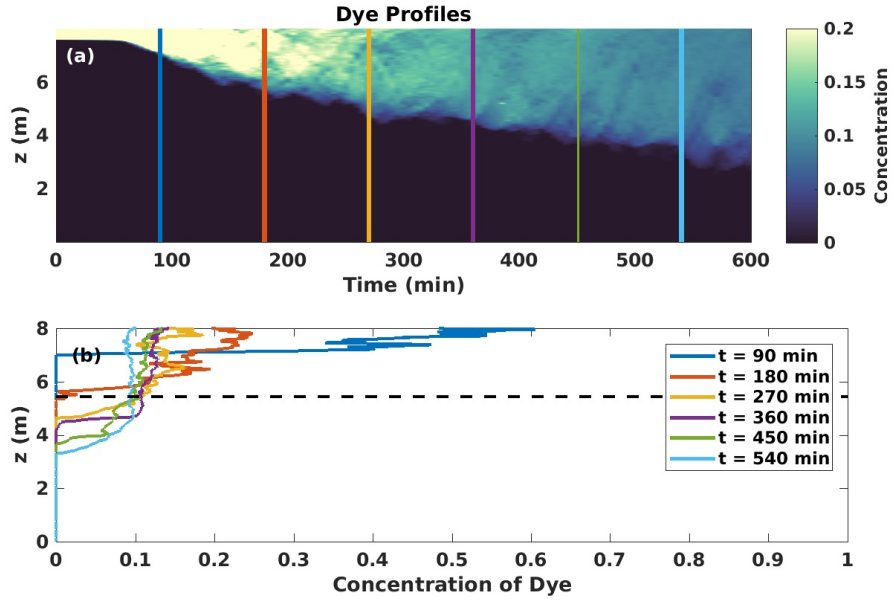

Figure 3.16: (a) Horizontal average of the dye field as a function of z and t in Lake Onego for the case of linear stratification. Note that the vertical axis is positive upwards. Coloured lines overlying the dye profiles correspond to the times displayed in the panels of the 2D evolution plots (i.e. vertical lines mark the passage of 90 minute intervals). (b) The concentration of dye as a function of z for the various times (indicated by colour) highlighted in panel (a). The dashed line outlines the extent of the photic zone for Lake Onego. For all times after $t = 180$ min, some concentration of the dye dives below this boundary.

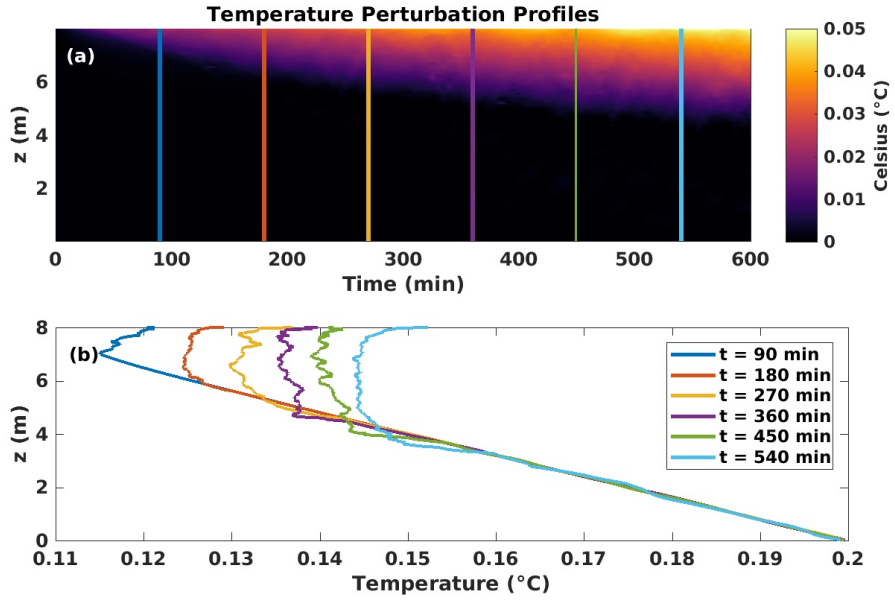

Figure 3.17: (a) Horizontal average of the temperature field as a function of z and t in Lake Onego for the case of linear stratification. The background stratification has been subtracted off to best display the heating effects of radiatively driven convection. Coloured lines overlying the temperature profiles correspond to the times displayed in the panels of the 2D evolution plots (i.e. vertical lines mark the passage of 90 minute intervals). (b) Stratification profiles corresponding to the various times (indicated by colour) shown in panel (a). At late times, we see the development of a nearly isothermal region extend below a sharply decreasing surface layer of approximately unit height.

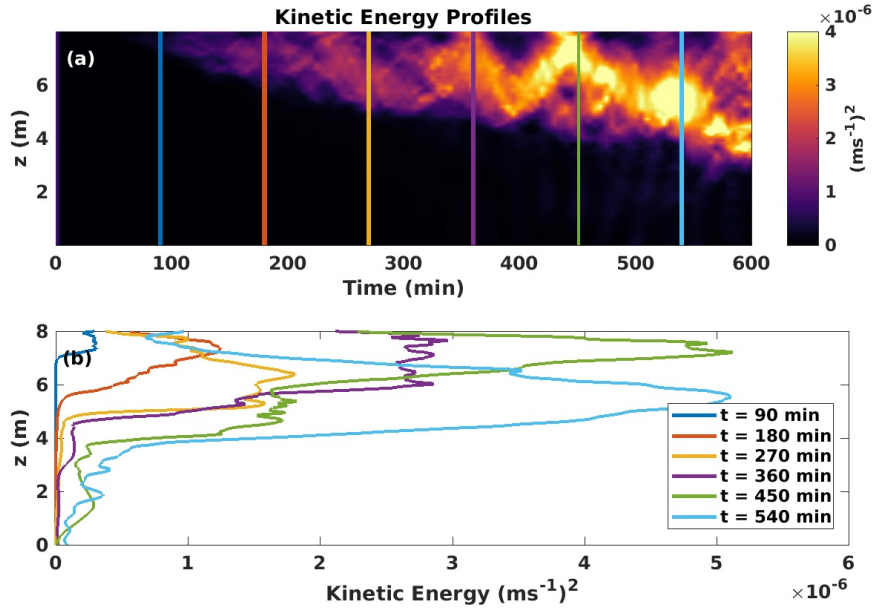

Figure 3.18: (a) Horizontal average of the kinetic energy as a function of z and t in Lake Onego for the case of linear stratification. Coloured vertical lines mark the passage of 90 minute intervals. Motion persists in the upper half of the domain starting shortly after $t = 90$ min, extending downwards at late times. (b) Kinetic energy profiles corresponding to the various times (indicated by colour) as shown in panel (a). At $t = 540$ min, the kinetic energy is centered slightly below the three-quarter mark of the domain.

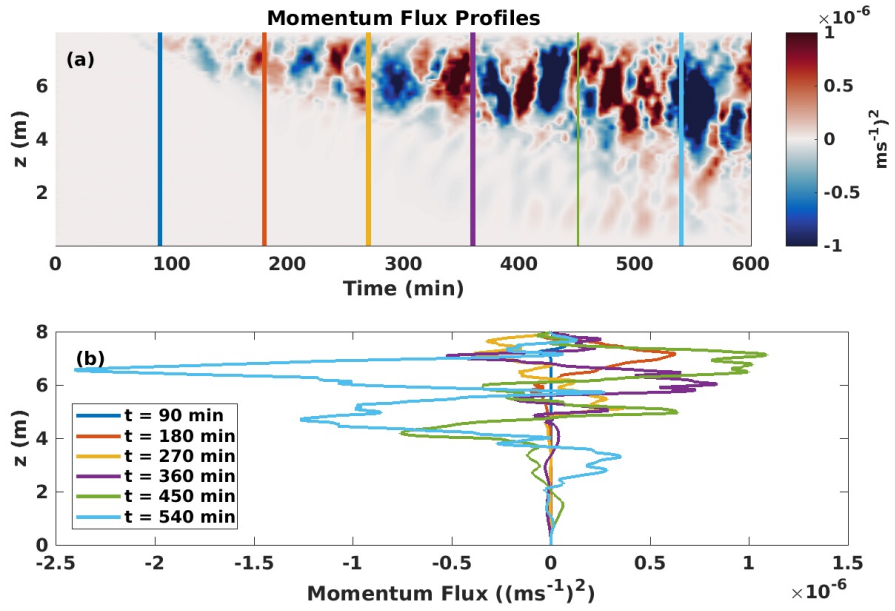

Figure 3.19: (a) Horizontal average of the momentum flux as a function of z and t in Lake Onego for the case of linear stratification. Coloured vertical lines mark the passage of 90 minute intervals. Note the transfer of momentum into the lower stratified layer at late times (most prominent after $t = 450$ min). (b) Momentum flux profiles corresponding to the various times (indicated by colour) as shown in panel (a). On average, the momentum flux is dominated by positive values, where a shift in this behaviour begins around $t = 540$ min.

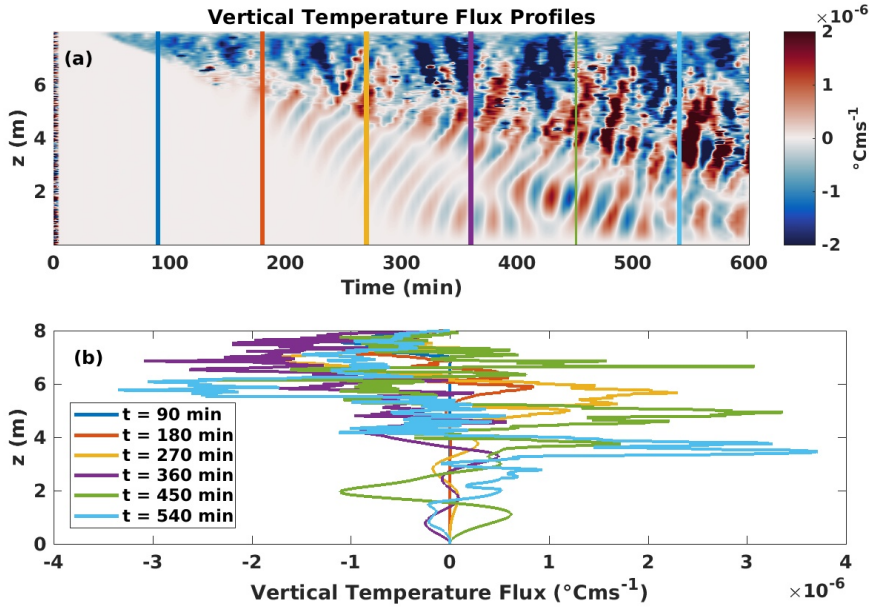

Figure 3.20: (a) Horizontal average of the vertical temperature flux as a function of z and t in Lake Onego for the case of linear stratification. Coloured vertical lines mark the passage of 90 minute intervals. There is a noticeably different structure in the upper convective zone than in the layer below. (b) Vertical temperature flux profiles corresponding to the various times (indicated by colour) as shown in panel (a). The temperature flux alternates between positive and negative values for all times after roughly $t = 175$ min.

3.3 Increased Radiation

We have now identified variations in under-ice radiatively driven convection introduced by differing attenuation lengths. Next, we investigate the effects of incoming solar radiation on the physical and biological processes as occur in both Lake Erie and Lake Onego during late winter (early spring). To be consistent with the results as presented above, we keep the same linear stratification profile and attenuation constants, only now, we increase the under-ice irradiance to double its previous value, such that $I_0 = 20$ Wm^{-2}. Note that an increase in under-ice irradiance is consistent with reduced albedo. Recall that the albedo depends on both the thickness and type of ice cover, as well as any snow that blankets its surface. Hence, a reduction in albedo could be consistent with less ice and/or snow-cover in the late winter months. The particular details surrounding the increase in I_0 are not important, but rather, the effects this change has on coupled bio-physical lake processes are. At this time, we remain focused on dynamics that occur while forcing is present. That is, simulations for this case are ran for the familiar 600 minutes (10 hours).

Figure 3.21 shows the time series of the fraction of dye remaining in the photic zone of Lake Erie and Lake Onego (on the same subplot) for differing values of incoming solar radiation. The under-ice irradiance values are $I_0 = 10$ Wm^{-2} and $I_0 = 20$ Wm^{-2} for panels (a) and (b), respectively. In panel (a), we see that no diatoms are lost to inhospitable depths in Lake Erie, as the fraction of dye retains its maximum value for the extent of the simulation. In contrast, diatoms exit the photic zone of Lake Onego starting at $t = 200$ min, and continue to decrease until $t = 580$min at which time a slight increase in the concentration of dye is observed. Despite this small uptake, more than one-third of the total diatom population is eliminated from the photic zone of Lake Onego.

Turning our attention now to panel (b) of Figure 3.21, we see a similar pattern in that diatoms are relatively safe in Lake Erie but suffer in the CDOM dominated waters of Lake Onego. Increasing the subsurface irradiance, I_0, by a factor of two shifts the elimination of phytoplankton to earlier times. For example, in Lake Onego, diatoms are removed from the photic zone roughly 75 minutes earlier as compared to their exodus in panel (a). However, the total fraction of dye remaining in the photic zone at the end of the simulation saturates close to the same value. That is, doubling I_0 only results in a further 10% loss of phytoplankton for lakes with high CDOM levels. Perhaps most interesting, is that in panel (b), Lake Erie does experience some diatom loss around $t = 560$ min. Although less than 10%, this loss is notable and hence significant. This implies that overall, the effects of increased radiation are damaging to diatom populations residing under ice cover, with more drastic implications existing for lakes with increased CDOM levels.

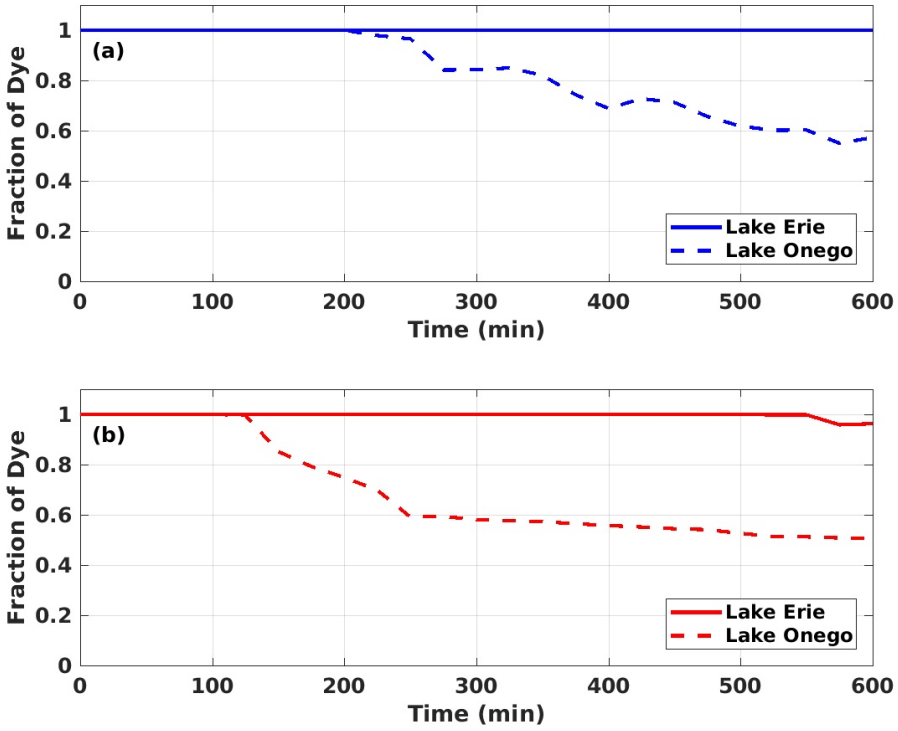

Figure 3.21: Time series of the fraction of dye remaining in the photic zone of Lake Erie and Lake Onego, respectively, for values of (a) $I_0 = 10$ Wm^{-2} and (b) $I_0 = 20$ Wm^{-2}. In both panels, Lake Onego has significantly less diatoms remaining in the photic zone as compared to Lake Erie. Increasing the subsurface irradiance by a factor of two shifts the elimination of phytoplankton to earlier times (roughly 75 minutes earlier in the case of Lake Onego), but the total fraction remaining at the end of the simulation saturates close to the same value. Note that in panel (b), Lake Erie does experience some diatom loss.

3.4 Diel Cycles

The last case we consider is that of diel cycles, where radiative forcing is effectively switched off after sunset. Here the timescale of the simulations encompass a 24 hour day, where 10 of these hours are subject to constant radiative forcing (see Equation 2.17) and the final 14 experience $I(z) = 0$. It is worth noting that the additional hours are simply appended to the previous case of linear stratification for Lake Erie and Lake Onego. That is, the linear stratification profile, attenuation coefficients, and under-ice irradiance, I_0, (experienced during day-time forcing) are the same for both cases; this is most clearly outlined in Table 2.2. While a sudden switch to non-zero forcing at sunset is not the most realistic assumption (day transitions to night gradually), it was the simplest scenario to apply to our model (SPINS). We leave the idea of temporal variability in external forcing as a suggestion for future work in the Conclusions section.

The relevant quantity to consider for diel dynamics is the kinetic energy. Although radiative forcing ceases at night, convective motions continue, unforced, beneath the ice surface until frictional damping dissipates the generated kinetic energy. The time required to damp these convective motions is assumed equal to the ratio of the (turbulent) kinetic energy to the rate of dissipation of this kinetic energy by friction ([19], [33]). In the literature, this ratio, or rather the time scale for frictional damping, is determined via scaling relationships. In this work, we simulate the under-ice dynamics and approximate the time at which convective motions cease based on analysis of the results (see detailed discussion below).

In Figure 3.22, panel (a), we see the horizontal average of the kinetic energy as a function of z and t for Lake Erie. Up until $t = 600$ min, the dynamics are exactly those displayed in Figure 3.10 (a), which considered constant day-time radiative forcing. After this time, however, radiative forcing is switched off, and we are able to evaluate how long it takes for frictional damping to dissipate the kinetic energy generated during the day. Note that because the simulations were ran for over twice as long as compared to the case of linear stratification (which considered day-time dynamics only), the vertical coloured lines mark the passage of 210 minutes intervals rather than the previous 90 minutes. Following the $t = 600$ min mark, it takes approximately 300 minutes for the kinetic energy to be effectively reduced to zero in the upper metre of the water column. Forrest et al. [19] determined the time required to halt motions associated with radiatively driven convection as approximately 78 minutes in Pavilion Lake (British Columbia, Canada). A similar timescale of 60 minutes was quoted by Kelley [33] for Lake Baikal (Russia). Both studies employed turbulence scaling theories to estimate these quoted values (see Equation 9 in [19], and Equation 7 in [33]). While a direct comparison is perhaps not completely accurate

given the difference in sites considered, our approximate value of 300 minutes for the damping timescale is much larger than either of those found in the studies listed here. Thus, it would appear that scaling relationships underestimate the time required for frictional damping to dissipate kinetic energy. However, a detailed comparison between methods (scaling relationships versus numerical simulations) requires additional study. Further to this, although motion in the surface layer stops at roughly $t = 900$ min, the kinetic energy adopts non-zero values across a significant portion of the domain following this time, particularly, in a 3 m thick region beneath the surface layer. This phenomenon is more clear in panel (b), where we see that even at late times ($t = 1260$ min), there are still significant regions of activity centred near 6 m and again at 3 m on the vertical axis. Hence, it would appear that the effects associated with frictional damping are not consistent over the entire vertical extent of the domain implying this is the case in lakes as well.

Figure 3.23 (a) considers the kinetic energy dynamics associated with Lake Onego. As with Lake Erie, the forcing stops at $t = 600$ min and prior to this time, the kinetic energy profile exacts that shown in Figure 3.18. Most interesting with Lake Onego is that after approximately 50 minutes without radiative forcing, the kinetic energy splits into three distinct regions. That is, the upper surface layer is dominated by strong values of kinetic energy, followed by an essentially motionless region, which lies above another persistent, though slightly less active layer than that observed at the surface. This implies that lakes with increased light attenuation (due to high CDOM levels) do not adopt anything close to a quiescent state following sunset. If we were to approximate the time at which convective motions cease, we could say that centered around 5.5 m above the bottom of the domain, it takes approximately 100 minutes for frictional damping to have any effect. However, this statement is quite weak given the outstanding dynamics visible in panel (b). All curves displayed exhibit considerable motion over some portion of the domain. Hence, to compare Lake Onego to either Lake Baikal or Pavilion Lake as we did above is not qualitative at best.

To increase our understanding of how the cessation of convective motions following sunset influences under-ice processes, we consider the time series of the fraction of dye remaining in the photic zone over the course of an entire day, for both Lake Erie and Lake Onego. In theory, as convective motions slow (or discontinue), diatoms will effectively lose the suspension mechanism responsible for keeping them within the photic zone; this is, of course, provided that other motions are unable to afford them with access to adequate light. The kinetic energy dynamics presented above imply that some motions continue past the point at which radiative forcing is turned off for both lakes. Based on this, we should observe that diatoms are able to remain suspended during the night with little effects on their overall concentration; Figure 3.24 shows exactly that. As we saw earlier in Figure 3.21

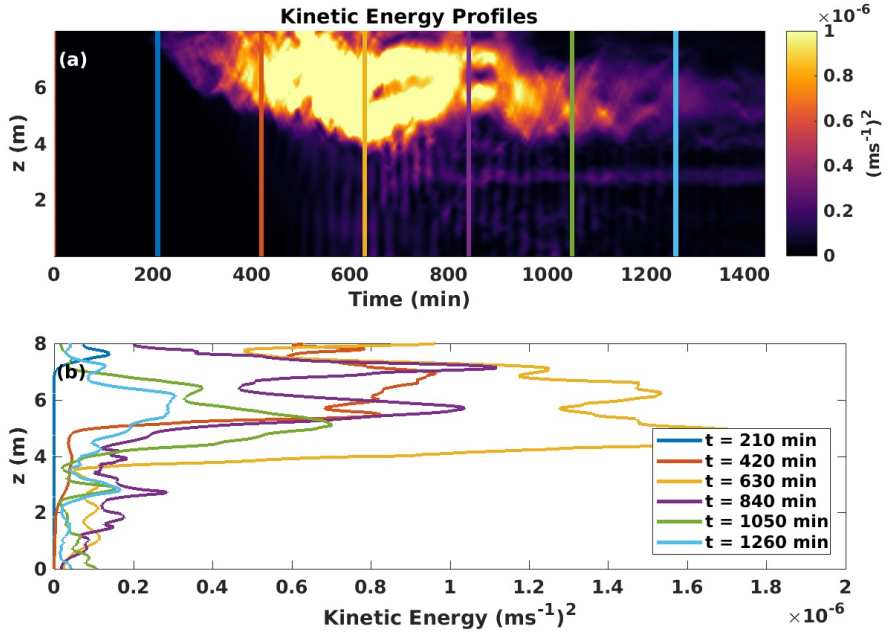

Figure 3.22: (a) Horizontal average of the kinetic energy as a function of z and t in Lake Erie for the case of diel cycles. Coloured vertical lines mark the passage of 210 minute intervals. Motion persists in the upper half of the domain starting shortly after $t = 210$ min, extending downwards at late times. Motion in the surface layer stops at roughly $t = 900$ min, but persists in a 3 m thick region beneath the surface layer. (b) Kinetic energy profiles corresponding to the various times (indicated by colour) as shown in panel (a).

(a), diatoms exit the photic zone of Lake Onego starting at $t = 200$ min and continue to decrease until just shy of the $t = 600$ min mark. We see these same dynamics here, but note that after $t = 600$ min (the time at which radiative forcing stops) no more diatoms are transported out of the photic zone. Hence, irrespective of whether we consider day, or both day and night, the same fraction of the population of diatoms (roughly one-third) is lost in Lake Onego. Similarly, the effects associated with with zero night-time forcing make no difference to diatoms in Lake Erie. As before, no phytoplankton are forced out of the photic zone over the course of the simulation.

Based on the results above, it would appear that diurnal variation in radiative forcing has no apparent effect on diatom species in the water column, or rather, that motions generated during the day are enough to keep phytoplankton in suspension at night. This

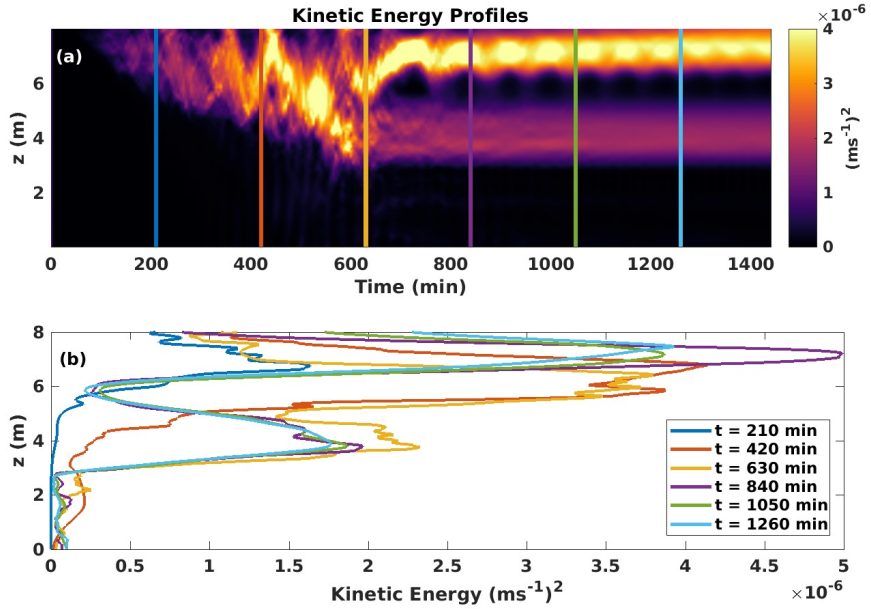

Figure 3.23: (a) Horizontal average of the kinetic energy as a function of z and t in Lake Onego for the case of diel cycles. Coloured vertical lines mark the passage of 210 minute intervals. At $t = 630$ min, the dominant kinetic energy splits into two distinct regions with a larger excitation seen in the near-surface layer. (b) Kinetic energy profiles corresponding to the various times (indicated by colour) as shown in panel (a). Note again the separation of kinetic energy into two distinct regions within the domain.

finding contradicts the conclusion of Kelley [33] that algal cells (phytoplankton) will fall to depths past those at which they are able to survive during the non-convective hours of the night. Note that Kelley [33] assumes that no other fluid motions are present and does assign a still-water sinking rate to phytoplankton species. As evidenced above, the first assumption is incorrect given the observed motions (however insignificant) over the vertical extent of the domain (see Figures 3.22 and 3.23). The second assumption of a still-water sinking speed, while valid, differs from that made in this thesis. Recall from the Methods section that we refrained from modelling the sinking behaviour of diatoms given that the vertical (convective) velocities were found to be a few orders of magnitude larger than the associated sinking speeds of *Aulacoseira islandica* ($\approx 10^{-6}$ ms^{-1}). This assumption holds for the case of the diel cycles where the convective velocities, though smaller than during the day, were still two orders of magnitude greater and hence would fully entrain diatoms in the water column.

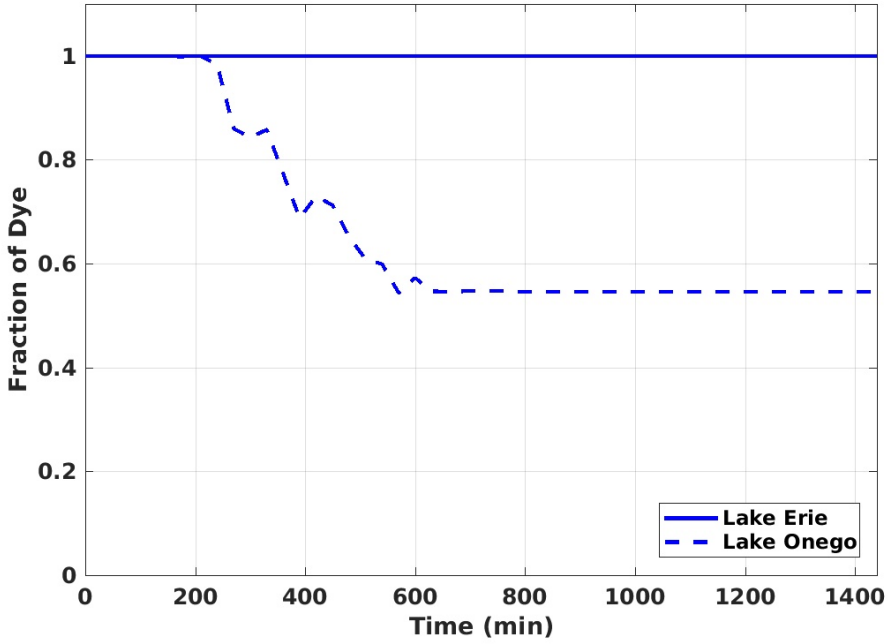

Figure 3.24: Time series of the fraction of dye remaining in the photic zone of Lake Erie and Lake Onego, respectively, over the course of 24 hours. The diel cycles consider the same linear stratification as before. After $t = 600$min, the time at which radiative forcing stops, no more diatoms are transported out of the photic zone in Lake Onego. Note that Lake Erie loses no phytoplankton over the course of the simulation.

Having now considered all cases as outlined in this thesis, we may briefly discuss the relevant dimensionless parameters. A natural length scale is given by the radiative scale of each lake, $L = L_{I(z)}$ (see Figure 2.3). If we choose, somewhat arbitrarily, the value for which light is reduced to 25% of its surface value, $L_{I(z)} = 1.3$ m for Lake Erie, and $L_{I(z)} = 0.75$ m for Lake Onego. In theory, these differing length scales would allow a dimensionless number to be defined for each lake. For this back of the envelope calculation, we restrict our attention to order of magnitude and simply take $L = L_{I(z)} \approx 1.0$ m for both lakes. A natural velocity scale is given by the convective (vertical) velocity, where we consider those experienced during the day when radiative forcing is present. This amounts to choosing $U = w \approx 10^{-3}$ ms^{-1} (consistent with the case of linear stratification). Note that we choose this scaling for U rather than the reduced night-time velocities associated with the diel cycles ($\approx 10^{-4}$ ms^{-1}) to consider the upper limit of all dimensionless quantities. With

these parameters specified, we may define the Reynolds number as

$$Re = \frac{UL}{\nu} \approx 10^3$$

where Re gives the ratio of inertia to viscous terms. Scaling thus suggests that the flow is transitional, but not fully turbulent under ice cover in the late winter (early spring). Accordingly, the turbulent scalings frequently applied in the RDC literature (see, for example, [43], [32]) are not strictly valid under the ice due to the low Reynolds number of flow therein. Hence, we stress that fully turbulent phenomenology should not be sought to explain under-ice processes. Perhaps the most important dimensionless quantity to consider for radiatively driven convection is the Grashof number. The Grashof number, Gr, gives the ratio between buoyancy and viscous terms and is estimated as

$$Gr = \frac{\Delta\rho g L^2}{\nu U}$$

where $\Delta\rho$ is a typical, dimensionless density difference. In our simulations, $\Delta\rho \approx 10^{-4}$. Using the length scales as defined above, we find $Gr \sim 10^7$ meaning that during the period of vigorous convection, buoyancy effects dominate viscous effects.

Chapter 4

Conclusions and Future Work

In this thesis, we have used a three band radiation model to drive an incompressible, stratified Navier Stokes model (SPINS) and thereby quantify the effects of radiatively driven convection under ice cover in late winter (early spring). Ice cover largely impacts the underlying physical processes of lakes, which in turn influences the ecosystem processes. The physical processes of greatest interest tend to center around the dynamics of temperature, light, and mixing, all of which have direct implications for primary producers. We consider four cases to identify how changes to the initial temperature stratification and the under-ice irradiance (light levels) affect physical processes occurring within the water column over different time scales. Two different geographical sites were considered, Lake Erie and Lake Onego, where the latter serves to highlight the effects of increased CDOM levels on light attenuation and subsequently under-ice convective mixing processes. Particular focus was given to the distribution of phytoplankton (diatoms) throughout the water column for all cases. Simulations were performed with the pseudo spectral incompressible Navier-Stokes solver (SPINS) in its DNS configuration [53].

Radiatively driven convection leads to a relatively well-mixed surface layer that increases in depth and penetrates into the stably stratified layer below. The case with no stratification proved to be somewhat unrealistic in that the developing mixed layer reached the model domain bottom after a short period of time (5 hours). Hence, we restricted our analysis of the under-ice dynamics to only one site for this case, that being Lake Erie, and quickly moved onto the more representative assumption of a linear background stratification. Here we found that the development of the convective mixed layer was consistent with an increase in depth and temperature during the day, where such behaviour was observed for both lakes. The rate of mixed layer deepening was slightly faster in Lake Onego (by roughly 30%), where convective motions begin up to 150 minutes sooner than

in Lake Erie. Additionally heat contributions to the water column (associated with radiatively driven convection) were more pronounced in Lake Onego. Considering for the moment only Lake Erie, we found that the relatively slow descent of the convective mixed layer (0.11 mms^{-1}) combined with the fact that it did not impinge upon the photic zone, was enough to keep diatoms in a region with significant access to light over the course of the simulation. This contrasts with the unstratified case, for which diatoms are reduced to less than two-thirds of their initial population shortly after convection sets in. Hence, one mechanism responsible for controlling the speed of diatom descent is the pre-existing under-ice stratification.

Another mechanism influencing diatom development is the amount of coloured dissolved organic matter (CDOM) present in the water column. The importance of light for phytoplankton development in lakes is well known, as is the critical role of mixing depth. However, light also plays a prominent role among factors that can limit under-ice phytoplankton growth. For example, increased CDOM levels as observed in Lake Onego, increase light absorption in the upper water column thereby limiting the depth of the photic zone. As calculated in this work, the vertical extent of the photic zone in Lake Onego is less than half that observed in Lake Erie. In Lake Onego, we found that the effect of convection was primarily negative by driving diatoms well below the shallow photic zone. The reduction of diatom concentration to less than two-thirds of its initial value is not unique to the case of no stratification as similar losses were observed in a linearly stratified Lake Onego, albeit over longer time scales (ten hours rather than five). Furthermore, we found that the effects of increased radiation, or under-ice irradiance, were damaging to diatom populations in both lakes with more drastic implications existing for Lake Onego. Thus, diatoms suffered considerably more in Lake Onego than in Lake Erie for the case of linear stratification and increased radiation. As a result of climate change, CDOM levels are on the rise in Lake Erie [14]. Thus, the negative effects on phytoplankton development as experienced in Lake Onego could soon be realized for this more local water body as well.

Radiatively driven convective is a diurnally intermittent process, meaning instabilities are only actively generated during the day. Considering the case of diel cycles, we found that the kinetic energy in both lakes persisted in localized regions over the domain extent throughout the night. Most notable, was that lakes with increased light attenuation (due to high CDOM levels) do not adopt anything close to a quiescent state following sunset, contradicting the general assumption in the literature. Furthermore, we found that scaling relationships frequently employed in studies of radiatively driven convection ([19], [33]) underestimate the time required for frictional damping to dissipate kinetic energy. Based on our results, we were able to conclude that motions generated during the day were enough to keep diatoms within the photic zone following sunset, irrespective of the lake considered.

Hence the diurnal variation in radiative forcing leaves diatom concentrations in the water column unaffected when one considers short time scales, such as those in our simulations.

As evidenced by this work, small differences in water temperatures (affecting stratification profiles) and weather conditions (affecting irradiance levels) can cause significant variations to under-ice fluid processes that impact phytoplankton development. This observed sensitivity of hydrodynamics in the late winter/early spring implies that climate change is likely to affect under-ice mixing regimes. Given that diatoms are heavily reliant on mixing, the physical dynamics of the water column are extremely important to their survival. Winter conditions determine proceeding phytoplankton populations and as such, changes to the mixing and circulation regimes under ice cover may alter blooms in the subsequent open water seasons ([39], [24], [50]). As long-term climate change alters environmental conditions, with effects cascading between seasons, it becomes increasingly important to enhance our understanding of the coupled bio-physical processes occurring under ice cover in the late winter months.

Future work should consider spatial and temporal variability in radiative forcing. Spatial variation would reflect differences in albedo across the ice-surface, for example, caused by regions which experience higher snow fall than others. Temporal variability in solar forcing would more realistically account for changes in weather conditions and light levels throughout the day. Amongst the simplest of suggestions is an increase in domain size and subsequent resolution. Similarly, lengthened time scales that observe dynamics over several diel cycles would enhance our understanding of the coupled processes occurring in the under-ice environment. Note that the consideration of longer time scales may require that the growth and population dynamics of winter diatoms be modelled. Further to this, three dimensional simulations would allow for a deeper exploration of feature organization in radiatively driven convection. All of these suggestions require significant computational resources and time, but are otherwise easy to implement in the current model.

Applied future work should attempt to extract more recent measurements of optical parameters from field data. In addition to the modified absorption spectrum of CDOM dominated water, the distribution of the radiative flux throughout the water column can be further modified by the primary producers within [33]. Thus, the effect that the concentration of phytoplankton has on water column heating is another clear avenue for future work. This added level of complexity would require that the radiative forcing term include plankton dependency, namely, $I(z, P)$. At present, the non-hydrostatic model (SPINS) used in this thesis cannot handle dye (phytoplankton) dependency while solving the coupled Navier-Stokes and heat equations. Hence, this is a substantial suggestion for future work but one that more clearly reflects all processes involved and could serve as representative model for other coupled process studies.

Bibliography

[1] Rita Adrian, Norbert Walz, Thomas Hintze, Sigrid Hoeg, and Renate Rusche. Effects of ice duration on plankton succession during spring in a shallow polymictic lake. *Freshwater Biology*, 41(3):621–634, 1999. ISSN 00465070. doi: 10.1046/j.1365-2427.1999.00411.x.

[2] Rita Adrian, Catherine M. O'Reilly, Horacio Zagarese, Stephen B Baines, Dag O. Hessen, Wendel Keller, David M. Livingstone, Ruben Sommaruga, Dietmar Straile, Ellen Van Donk, Gesa A. Weyhenmeyer, and Monika Winder. Lakes as sentinels of climate change. *Limnology and Oceanography*, 54(6, part 2):2283–2297, 2009.

[3] Kevin R. Arrigo and David N. Thomas. Large scale importance of sea ice biology in the Southern Ocean. *Antarctic Science*, 16(4):471–486, 2004. ISSN 09541020. doi: 10.1017/S0954102004002263.

[4] Lars Bengtsson. Mixing in ice-covered lakes. *Hydrobiologia*, 322(1-3):91–97, 1996. ISSN 00188158. doi: 10.1007/BF00031811.

[5] Stefan Bertilsson, Amy Burgin, Cayelan C. Carey, Samuel B. Fey, Hans Peter Grossart, Lorena M. Grubisic, Ian D. Jones, Georgiy Kirillin, Jay T. Lennon, Ashley Shade, and Robyn L. Smyth. The under-ice microbiome of seasonally frozen lakes. *Limnology and Oceanography*, 58(6):1998–2012, 2013. ISSN 00243590. doi: 10.4319/lo.2013.58.6.1998.

[6] S. J. Bolsenga. Radiation transmittance through lake ice in the 400-700m range. *Journal of Glaciology*, 27(95):57–66, 1981. ISSN 00221430. doi: 10.1017/s0022143000011229.

[7] S. J. Bolsenga and H. A. Vanderploeg. Estimating photosynthetically available radiation into open and ice-covered freshwater lakes from surface characteristics; a high transmittance case study. *Hydrobiologia*, 243-244(1):95–104, 1992. ISSN 00188158. doi: 10.1007/BF00007024.

[8] Damien Bouffard and Alfred Wüest. Convection in Lakes. *Annual Review of Fluid Mechanics*, 51(1):189–215, 2019. ISSN 0066-4189. doi: 10.1146/annurev-fluid-010518-040506.

[9] Damien Bouffard, Galina Zdorovennova, Sergey Bogdanov, Tatyana Efremova, Sébastien Lavanchy, Nikolay Palshin, Arkady Terzhevik, Love Råman Vinnå, Sergey Volkov, Alfred Wüest, Roman Zdorovennov, and Hugo N. Ulloa. Under-ice convection dynamics in a boreal lake. *Inland Waters*, 9(2):142–161, 2019.

[10] Brett F. Branco and Thomas Torgersen. Predicting the onset of thermal stratification in shallow inland waterbodies. *Aquatic Sciences*, 71:65–79, 2009. doi: 10.1007/s00027-009-8063-3.

[11] Denise A. Bruesewitz, Cayelan C. Carey, David C. Richardson, and Kathleen C. Weathers. Under-ice thermal stratification dynamics of a large, deep lake revealed by high-frequency data. *Limnology and Oceanography*, 60(2):347–359, 2015. ISSN 19395590. doi: 10.1002/lno.10014.

[12] David Brydon. A new approximation of the equation of state for seawater, suitable for numerical ocean models. *Journal of Geophysical Research*, 104(1):1537–1540, 1999.

[13] Alicia Cortés and Sally Macintyre. Mixing processes in small arctic lakes during spring. *Limnology and Oceanography*, 65:260–288, 2020. doi: 10.1002/lno.11296.

[14] Rose M. Cory, Timothy W. Davis, Gregory J. Dick, Thomas Johengen, Vincent J. Denef, Michelle A. Berry, Sarah E. Page, Susan B. Watson, Kate Yuhas, and George W. Kling. Seasonal dynamics in dissolved organic matter, hydrogen peroxide, and cyanobacterial blooms in Lake Erie. *Frontiers in Marine Science*, 3:1–17, 2016. ISSN 22967745. doi: 10.3389/fmars.2016.00054.

[15] Louis Alexandre Couston. Turbulent convection in subglacial lakes. *Journal of Fluid Mechanics*, 915, 2021. ISSN 14697645. doi: 10.1017/jfm.2021.38.

[16] Irena F. Creed, Ann Kristin Bergström, Charles G. Trick, Nancy B. Grimm, Dag O. Hessen, Jan Karlsson, Karen A. Kidd, Emma Kritzberg, Diane M. McKnight, Erika C. Freeman, Oscar E. Senar, Agneta Andersson, Jenny Ask, Martin Berggren, Mehdi Cherif, Reiner Giesler, Erin R. Hotchkiss, Pirkko Kortelainen, Monica M. Palta, Tobias Vrede, and Gesa A. Weyhenmeyer. Global change-driven effects on dissolved organic matter composition: Implications for food webs of northern lakes. *Global Change Biology*, 24(8):3692–3714, 2018. ISSN 13652486. doi: 10.1111/gcb.14129.

[17] Sebastian Diehl. Phytoplankton , Light , and Nutrients in a Gradient of Mixing Depths : Theory. *Ecology*, 83(2):386–398, 2002.

[18] David M. Farmer. Penetrative convection in the absence of mean shear. *Quarterly Journal of the Royal Meteorological Society*, 101(430):869–891, 1975. ISSN 1477870X. doi: 10.1002/qj.49710143011.

[19] Alexander L. Forrest, Bernard E. Laval, Roger Pieters, and Darlene S.S. Lim. Convectively driven transport in temperate lakes. *Limnology and Oceanography*, 53(5 PART 2):2321–2332, 2008. ISSN 00243590. doi: 10.4319/lo.2008.53.5{_}part{_}2.2321.

[20] Marina Gerea, Gonzalo L. Pérez, Fernando Unrein, Carolina Soto Cárdenas, Donald Morris, and Claudia Queimaliños. CDOM and the underwater light climate in two shallow North Patagonian lakes: evaluating the effects on nano and microphytoplankton community structure. *Aquatic Sciences*, 79(2):231–248, 2017. ISSN 14209055. doi: 10.1007/s00027-016-0493-0.

[21] N. G. Granin, D. H. Jewson, R. Yu. Gnatovsky, L. A. Levin, A. A. Zhdanov, L. A. Gorbunova, V. V. Tsekhanovsky, L. M. Doroschenko, and N. Yu. Mogilev. Turbulent mixing under ice and the growth of diatoms in Lake Baikal. *Internationale Vereinigung für theoretische und angewandte Limnologie: Verhandlungen*, 27(5):2812–2814, 2000. doi: 10.1080/03680770.1998.11898179.

[22] Stephanie E Hampton, Derek K Gray, Lyubov R Izmest, Marianne V Moore, and Tedy Ozersky. The Rise and Fall of Plankton : Long-Term Changes in the Vertical Distribution of Algae and Grazers in Lake Baikal , Siberia. *PLOS One*, 9(2):e88920, 2014. doi: 10.1371/journal.pone.0088920.

[23] Stephanie E. Hampton, Marianne V. Moore, Tedy Ozersky, Emily H. Stanley, Christopher M. Polashenski, and Aaron W.E. Galloway. Heating up a cold subject: Prospects for under-ice plankton research in lakes. *Journal of Plankton Research*, 37(2):277–284, 2015. ISSN 14643774. doi: 10.1093/plankt/fbv002.

[24] Stephanie E. Hampton, Aaron W.E. Galloway, Stephen M. Powers, Ted Ozersky, Kara H. Woo, Ryan D. Batt, Stephanie G. Labou, Catherine M. O'Reilly, Sapna Sharma, Noah R. Lottig, Emily H. Stanley, Rebecca L. North, Jason D. Stockwell, Rita Adrian, Gesa A. Weyhenmeyer, Lauri Arvola, Helen M. Baulch, Isabella Bertani, Larry L. Bowman, Cayelan C. Carey, Jordi Catalan, William Colom-Montero, Leah M. Domine, Marisol Felip, Ignacio Granados, Corinna Gries, Hans Peter Grossart, Juta Haberman, Marina Haldna, Brian Hayden, Scott N. Higgins, Jeff C. Jolley, Kimmo K.

Kahilainen, Enn Kaup, Michael J. Kehoe, Sally MacIntyre, Anson W. Mackay, Heather L. Mariash, Robert M. McKay, Brigitte Nixdorf, Peeter Nõges, Tiina Nõges, Michelle Palmer, Don C. Pierson, David M. Post, Matthew J. Pruett, Milla Rautio, Jordan S. Read, Sarah L. Roberts, Jacqueline Rücker, Steven Sadro, Eugene A. Silow, Derek E. Smith, Robert W. Sterner, George E.A. Swann, Maxim A. Timofeyev, Manuel Toro, Michael R. Twiss, Richard J. Vogt, Susan B. Watson, Erika J. Whiteford, and Marguerite A. Xenopoulos. Ecology under lake ice. *Ecology Letters*, 20(1):98–111, 2017. ISSN 14610248. doi: 10.1111/ele.12699.

[25] E. Therese Harvey, Susanne Kratzer, and Agneta Andersson. Relationships between colored dissolved organic matter and dissolved organic carbon in different coastal gradients of the Baltic Sea. *Ambio*, 44(3):392–401, 2015. ISSN 00447447. doi: 10.1007/s13280-015-0658-4.

[26] Nathan Hawley, Dmitry Beletsky, and Jia Wang. Ice thickness measurements in Lake Erie during the winter of 2010–2011. *Journal of Great Lakes Research*, 44(3):388–397, 2018. ISSN 03801330. doi: 10.1016/j.jglr.2018.04.004. URL https://doi.org/10.1016/j.jglr.2018.04.004.

[27] A. J. Horne and C. R. Goldman. Understanding Lake Ecology. In *Lake Ecology Overview*, chapter 1. McGraw-Hill Co., New York, New York, USA., 2nd edition, 1994.

[28] Jef Huisman and Ben Sommeijer. Maximal sustainable sinking velocity of phytoplankton. *Marine Ecology Progress Series*, 244:39–48, 2002. ISSN 01718630. doi: 10.3354/meps244039.

[29] Jef Huisman, Jonathan Sharples, Jasper M. Stroom, Petra M. Visser, W. Edwin A. Kardinaal, Jolanda M.H. Verspagen, and Ben Sommeijer. Changes in turbulent mixing shift competition for light between phytoplankton species. *Ecology*, 85(11):2960–2970, 2004. ISSN 00129658. doi: 10.1890/03-0763.

[30] J. H. Jerome, R. P. Bukata, and J. E. Bruton. Spectral Attenuation and Irradiance in the Laurentian Great Lakes. *Journal of Great Lakes Research*, 9(1):60–68, 1983. ISSN 03801330. doi: 10.1016/S0380-1330(83)71872-1. URL http://dx.doi.org/10.1016/S0380-1330(83)71872-1.

[31] David H. Jewson, Nick G. Granin, Andre A. Zhdanov, and Ruslan Yu Gnatovsky. Effect of snow depth on under-ice irradiance and growth of Aulacoseira baicalensis in

Lake Baikal. *Aquatic Ecology*, 43(3):673–679, 2009. ISSN 13862588. doi: 10.1007/s10452-009-9267-2.

[32] Tobias Jonas, Adolf Stips, Werner Eugster, and Alfred Wüest. Observations of a quasi shear-free lacustrine convective boundary layer: Stratification and its implications on turbulence. *Journal of Geophysical Research C: Oceans*, 108(10):26–1, 2003. ISSN 01480227. doi: 10.1029/2002jc001440.

[33] Dan E. Kelley. Convection in ice-covered lakes: Effects on algal suspension. *Journal of Plankton Research*, 19(12):1859–1880, 1997. ISSN 01427873. doi: 10.1093/plankt/19.12.1859.

[34] Georgiy Kirillin, Matti Leppäranta, Arkady Terzhevik, Nikolai Granin, Juliane Bernhardt, Christof Engelhardt, Tatyana Efremova, Sergey Golosov, Nikolai Palshin, Pavel Sherstyankin, Galina Zdorovennova, and Roman Zdorovennov. Physics of seasonally ice-covered lakes: A review. *Aquatic Sciences*, 74(4):659–682, 2012. ISSN 10151621. doi: 10.1007/s00027-012-0279-y.

[35] Christopher A Klausmeier and Elena Litchman. Algal Games : The Vertical Distribution of Phytoplankton in Poorly Mixed Water Columns. *Limnology and Oceanography*, 46(8):1998–2007, 2001.

[36] Pijush K. Kundu. *Fluid Mechnaics*. Academic Press, Inc., 1990.

[37] Diane Lavoie, Kenneth Denman, and Christine Michel. Modeling ice algal growth and decline in a seasonally ice-covered region of the Arctic (Resolute Passage, Canadian Archipelago). *Journal of Geophysical Research*, 110:C11009, 2005. ISSN 21699291. doi: 10.1029/2005JC002922.

[38] Matti Leppäranta. *Freezing of Lakes and the Evolution of their Ice Cover*. Praxis Publishing Chichester, 2015.

[39] Karl Erich Lindenschmidt, Helen M. Baulch, and Emily Cavaliere. River and lake ice processes-Impacts of freshwater ice on aquatic ecosystems in a changing globe. *Water*, 10:1586, 2018. ISSN 20734441. doi: 10.3390/w10111586.

[40] John J Magnuson, Dale M Robertson, Barbara J Benson, Randolph H Wynne, David M Livingstone, Tadashi Arai, Raymond A Assel, Roger G Barry, Virginia Card, Esko Kuusisto, Nick G Granin, Terry D Prowse, Kenton M Stewart, and Valery S Vuglinksi. Historical Trends in Lake and River Ice Cover in the Northern Hemisphere. *Science*, 289:1743–1746, 2000.

[41] Octavia Mahdiyan, Alessandro Filazzola, Lewis A. Molot, Derek Gray, and Sapna Sharma. Drivers of water quality changes within the Laurentian Great Lakes region over the past 40 years. *Limnology and Oceanography*, 66(1):237–254, 2021. ISSN 19395590. doi: 10.1002/lno.11600.

[42] P. C. Matthews and S. I. Heaney. Solar heating and its influence on mixing in ice-covered lakes. *Freshwater Biology*, 18(1):135–149, 1987. ISSN 13652427. doi: 10.1111/j.1365-2427.1987.tb01302.x.

[43] Dmitrii Mironov, Arkady Terzhevik, Georgy Kirillin, Tobias Jonas, Joakim Malm, and David Farmer. Radiatively driven convection in ice-covered lakes: Observations, scaling, and a mixed layer model. *Journal of Geophysical Research*, 107:1–16, 2002. ISSN 0148-0227. doi: 10.1029/2001jc000892.

[44] Catherine M. O'Reilly, Sapna Sharma, Derek K. Gray, Stephanie E. Hampton, Jordan S. Read, Rex J. Rowley, Philipp Schneider, John D. Lenters, Peter B. McIntyre, Benjamin M. Kraemer, Gesa A. Weyhenmeyer, Dietmar Straile, Bo Dong, Rita Adrian, Mathew G. Allan, Orlane Anneville, Lauri Arvola, Jay Austin, John L. Bailey, Jill S. Baron, Justin D. Brookes, Elvira De Eyto, Martin T. Dokulil, David P. Hamilton, Karl Havens, Amy L. Hetherington, Scott N. Higgins, Simon Hook, Lyubov R. Izmest'Eva, Klaus D. Joehnk, Kulli Kangur, Peter Kasprzak, Michio Kumagai, Esko Kuusisto, George Leshkevich, David M. Livingstone, Sally MacIntyre, Linda May, John M. Melack, Doerthe C. Mueller-Navarra, Mikhail Naumenko, Peeter Noges, Tiina Noges, Ryan P. North, Pierre Denis Plisnier, Anna Rigosi, Alon Rimmer, Michela Rogora, Lars G. Rudstam, James A. Rusak, Nico Salmaso, Nihar R. Samal, Daniel E. Schindler, S. Geoffrey Schladow, Martin Schmid, Silke R. Schmidt, Eugene Silow, M. Evren Soylu, Katrin Teubner, Piet Verburg, Ari Voutilainen, Andrew Watkinson, Craig E. Williamson, and Guoqing Zhang. Rapid and highly variable warming of lake surface waters around the globe. *Geophysical Research Letters*, 42(24):10773–10781, 2015. ISSN 19448007. doi: 10.1002/2015GL066235.

[45] P Pernica, R L North, and H M Baulch. In the cold light of day : the potential importance of under-ice convective mixed layers to primary producers. *Inland Waters*, 7(2):138–150, 2017. ISSN 2044-2041. doi: 10.1080/20442041.2017.1296627. URL http://doi.org/10.1080/20442041.2017.1296627.

[46] M P Petrov, A Yu Terzhevik, N I Palshin, R E Zdorovennov, and G E Zdorovennova. Absorption of Solar Radiation by Snow-and-Ice Cover of Lakes. *Water Resources*, 32 (5):496–504, 2005.

[47] Colin Reynolds. *Ecology of Phytoplankton*. Cambridge University Press, 2006.

[48] E. J. Rochelle-Newall and T. R. Fisher. Chromophoric dissolved organic matter and dissolved organic carbon in Chesapeake Bay. *Marine Chemistry*, 77(1):23–41, 2002. ISSN 03044203. doi: 10.1016/S0304-4203(01)00073-1.

[49] Pauliina Salmi and Kalevi Salonen. Regular build-up of the spring phytoplankton maximum before ice-break in a boreal lake. *Limnology and Oceanography*, 61(1):240–253, 2016. ISSN 19395590. doi: 10.1002/lno.10214.

[50] Kalevi Salonen, Merja Pulkkanen, Pauliina Salmi, and Ross W. Griffiths. Interannual variability of circulation under spring ice in a boreal lake. *Limnology and Oceanography*, 59(6):2121–2132, 2014. ISSN 19395590. doi: 10.4319/lo.2014.59.6.2121.

[51] J. J. Simpson and T. D. Dickey. Alternative Parameterizations of Downward Irradiance and Their Dynamical Significance. *Journal of Physical Oceanography*, 11: 876–882, 1981.

[52] Ena Lucia Suarez, Marie Caroline Tiffay, Nataliia Kalinkina, Tatjana Tchekryzheva, Andrey Sharov, Elena Tekanova, Maria Syarki, Roman E. Zdorovennov, Elena Makarova, Evanthia Mantzouki, Patrick Venail, and Bastiaan W. Ibelings. Diurnal variation in the convection-driven vertical distribution of phytoplankton under ice and after ice-off in large Lake Onego (Russia). *Inland Waters*, 9(2):193–204, 2019. ISSN 2044205X. doi: 10.1080/20442041.2018.1559582.

[53] Christopher J. Subich, Kevin G. Lamb, and Marek Stastna. Simulation of the Navier-Stokes equations in three dimensions with a spectral collocation method. *International Journal for Numerical Methods in Fluids*, 73(2):103–129, 2013. ISSN 02712091. doi: 10.1002/fld.3788.

[54] M. R. Twiss, R. M.L. McKay, R. A. Bourbonniere, G. S. Bullerjahn, H. J. Carrick, R. E.H. Smith, J. G. Winter, N. A. D'souza, P. C. Furey, A. R. Lashaway, M. A. Saxton, and S. W. Wilhelm. Diatoms abound in ice-covered Lake Erie: An investigation of offshore winter limnology in Lake Erie over the period 2007 to 2010. *Journal of Great Lakes Research*, 38(1):18–30, 2012. ISSN 03801330. doi: 10.1016/j.jglr.2011.12.008. URL http://dx.doi.org/10.1016/j.jglr.2011.12.008.

[55] Hugo N. Ulloa, Alfred Wüest, and Damien Bouffard. Mechanical energy budget and mixing efficiency for a radiatively heated ice-covered waterbody. *Journal of Fluid Mechanics*, 852:R1–R13, 2018. ISSN 14697645. doi: 10.1017/jfm.2018.587.

[56] Hugo N. Ulloa, Kraig B. Winters, Alfred Wüest, and Damien Bouffard. Differential Heating Drives Downslope Flows that Accelerate Mixed-Layer Warming in Ice-Covered Waters. *Geophysical Research Letters*, 46:13872–13882, 2019. ISSN 19448007. doi: 10.1029/2019GL085258.

[57] Anu Vehmaa and Kalevi Salonen. Development of phytoplankton in Lake Pääjärvi (Finland) during under-ice convective mixing period. *Aquatic Ecology*, 43(3):693–705, 2009. ISSN 13862588. doi: 10.1007/s10452-009-9273-4.

[58] Sergey Volkov, Sergey Bogdanov, Roman Zdorovennov, Galina Zdorovennova, Arkady Terzhevik, Nicolay Palshin, Damien Bouffard, and Georgiy Kirillin. Fine scale structure of convective mixed layer in ice-covered lake. *Environmental Fluid Mechanics*, 19(3):751–764, 2019. ISSN 15731510. doi: 10.1007/s10652-018-9652-2. URL https://doi.org/10.1007/s10652-018-9652-2.

[59] Chelsea J. Weiskerger, Mark D. Rowe, Craig A. Stow, Dack Stuart, and Tom Johengen. Application of the Beer–Lambert Model to Attenuation of Photosynthetically Active Radiation in a Shallow, Eutrophic Lake. *Water Resources Research*, 54(11):8952–8962, 2018. ISSN 19447973. doi: 10.1029/2018WR023024.

[60] Monika Winder, John E. Reuter, and S. Geoffrey Schladow. Lake warming favours small-sized planktonic diatom species. *Proceedings of the Royal Society B: Biological Sciences*, 276(1656):427–435, 2009. ISSN 14712970. doi: 10.1098/rspb.2008.1200.

[61] Kraig B. Winters, Hugo N. Ulloa, Alfred Wüest, and Damien Bouffard. Energetics of Radiatively Heated Ice-Covered Lakes. *Geophysical Research Letters*, 46(15):8913–8925, 2019. ISSN 19448007. doi: 10.1029/2019GL084182.

[62] Alfred Wüest, Natacha Pasche, Bastiann W.Ibelings, Sapna Sharma, and Nikolay Filatov. Life under ice in Lake Onego (Russia) – an interdisciplinary winter limnology study. *Inland Waters*, 9(2):125–129, 2019.

[63] Bernard Yang, Joelle Young, Laura Brown, and Mathew Wells. High-Frequency Observations of Temperature and Dissolved Oxygen Reveal Under-Ice Convection in a Large Lake. *Geophysical Research Letters*, 44:218–12, 2017. ISSN 19448007. doi: 10.1002/2017GL075373.

[64] Bernard Yang, Mathew G. Wells, Jingzhi Li, and Joelle Young. Mixing, stratification, and plankton under lake-ice during winter in a large lake: Implications for spring dissolved oxygen levels. *Limnology and Oceanography*, 9999:1–17, 2020. ISSN 19395590. doi: 10.1002/lno.11543.

[65] Zhengzhen Zhou, Laodong Guo, and Elizabeth C. Minor. Characterization of bulk and chromophoric dissolved organic matter in the Laurentian Great Lakes during summer 2013, 2016. ISSN 03801330.